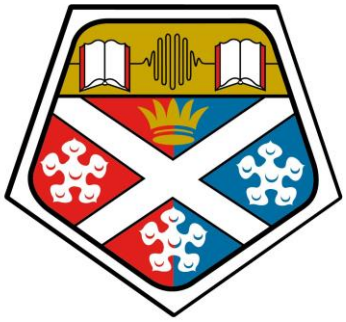

University of Strathclyde Glasgow

Design and Optimisation of a Type-C Tank for Liquid Hydrogen Marine Transport

By

Yinhua Liu

202288789

A THESIS

Submitted in partial fulfilment of the requirements for the degree of

MEng - Marine Engineering

UNIVERSITY OF STRATHCLYDE

Declaration

This thesis is the result of the author's original research. It has been composed by the author and has not been previously submitted for examination which has led to the award of a degree.

This thesis has been approved in partial fulfilment of the requirements for the Degree of MPhil in Marine Engineering, Department of Naval Architecture, Ocean & Marine Engineering.

Thesis Advisor: Peilin Zhou

Thesis Co-Advisor: Byongug Jeong

Student Name: Yinhua Liu

Signature: Date:

Acknowledgements

First of all, I would like to express my sincere gratitude to my supervisor, Professor Peilin Zhou. He has been an exceptional mentor, demonstrating remarkable responsibility and patience throughout my research. His invaluable guidance and support have not only helped me in my academic research but also in my personal life. I hold him in high regard as a true elder whom I will always respect and cherish.

I would also like to extend my thanks to the teachers and colleagues in the NAOME, especially Dr Haibin, Dr Zhiming Yuan and his research group members, and my roommate, Yulin. Their constant support and assistance have been essential to my academic and research pursuits.

My deep appreciation goes to my family, especially my parents, who have been unwavering in their support of my educational goals and aspirations. Their selfless dedication and encouragement have been instrumental in my study.

Lastly, I would like to express my sincere gratitude to my girlfriend, Shudan Yang. Our mutual inspiration and support have been invaluable to me, and her unwavering encouragement has been a constant source of strength. With her by my side, I am confident that we can overcome any obstacle and pursue a bright future together.

Table of Contents

Abstract

As one of the most promising renewable energy sources, hydrogen has the excellent environmental benefit of producing zero emissions. A key technical challenge in using hydrogen across sectors lies in its storage technology. The storage temperature of liquid hydrogen at atmospheric pressure is 20 K, or -253 °C, close to absolute zero, so the storage materials and the insulation layers are subjected to extremely stringent requirements regarding the cryogenic behaviour of the medium. In this context, this research proposed designing a large liquid hydrogen type-C tank, determining the material and thickness of the primary and secondary shells, and using Vapor-Cooled Shield (VCS) and Rigid Polyurethane Foams (RPF) as the insulation layer. A parametric study on the design of the insulation layer was carried out by establishing a thermodynamic model. The effects of VCS location on heat ingress to the liquid hydrogen transport tank and insulation temperature distribution when the VCS heat exchanger tubes were fed with self-evaporating hydrogen gas, forced-evaporating hydrogen gas and liquid hydrogen, respectively, were investigated. Finally, research outcomes suggested two optimal design schemes, respectively, for reducing the thickness of the insulation when the heat transfer rate was fixed and reducing the heat transfer rate when the thickness of the insulation was fixed.

Keywords: *liquid hydrogen transportation; Self-evaporation Vapor-Cooled Shield (SVCS); Forced-evaporation Vapor-Cooled Shield (FVCS); Cryogenic insulation; Type-C tank.*

List of Figures

List of Tables

1 Introduction

1.1 Background

As held in Egypt in November 2022, the 27th Conference of the Parties of the UNFCCC (COP 27) was focused on seeking effective ways to make consistent efforts to meet energy conservation and GHG emission reduction targets [1]. As a renewable energy source, hydrogen combustion not only has an extremely high calorific value (1.43×10^8 J/kg) - roughly three times that of gasoline (4.6×10^7 J/kg) at the same weight - but also emits no greenhouse gases or sulfides [2]. Thus, a large-scale development and utilization of hydrogen energy have been regarded as one of the most effective methods of reducing air pollution and the greenhouse effect. The European Union mandates that hydrogen energy must meet half of the European Union's basic energy demand by 2050 [3]. According to the HYDROGEN ROADMAP EUROPE report, Europe may need to generate approximately 2,250 terawatt-hours (TWh) of hydrogen per year by 2050 [4]. In addition, hydrogen energy is highly competitive in industries such as transportation and aerospace due to its efficient energy carrier properties [5-7].

Both gaseous and liquefied hydrogen are attracting a lots of research interests, especially for storage and transport. High-pressure compressed hydrogen is the most widely used method of hydrogen storage. It boasts high hydrogen fill and release rates. However, the large tank weight and small capacity of high-pressure cylinders make it a poor choice for transporting hydrogen over long distances and on a large scale. Gaseous hydrogen can be liquefied at one-atmosphere pressure and 20 K (-253 °C), and the density of liquid

hydrogen at one-atmosphere pressure is approximately 800 times that gaseous hydrogen. The high energy density and the ability to transport it in large tanks make liquid hydrogen more advantageous for mass transportation [8]. However, there is a significant temperature difference between liquid hydrogen and the ambient temperature (about 280 K), which makes heat transfer through the storage tank hull and evaporation loss unavoidable [9, 10]. The greatest challenging issue in liquid hydrogen transportation and storage technology is to minimize heat transfer into the cargo [11, 12]. Thus, it is difficult to realize the globalization of hydrogen energy and achieve a large-scale hydrogen energy transport across different regions around the world. In this regard, hydrogen transport by ship is undoubtedly considered as an excellent choice. In 2021, the world's first hydrogen transport ship, Suiso Frontier, began operating between Japan and Australia, using vacuum insulation and panel insulation to transport 2,500 m^3 (No.1 & No.2 tank: 1,250 m^3 each) of liquid hydrogen at a time [13, 14]. H. Park et al. [15] proposed a flexible vacuum membrane to aid in the vacuum insulation of medium-sized hydrogen storage tanks. A. N. Alkhaledi et al. [16] designed a liquid hydrogen carrier with four large type-C tanks based on an LNG carrier, using RPF for the insulation of the tanks. During the research and development of new ships, Japanese and Australian researchers discovered that vacuum insulation is not a viable option for a large cargo containment system due to the high costs involved in the construction of large internal vacuum tanks. A new design of cargo containment system should be used. To reduce heat transfer, it was found that it would be more advantageous to replace the vacuum and add a double insulation layer by filling the insulation layer with hydrogen to reduce heat transfer [17].

The Vapor-Cooled Shield (VCS) is a highly efficient thermal insulation device that can cool and insulate objects by using a cooling medium. It is widely used in the thermal protection of astronomical telescopes and space probes [10, 18-20]. The cooling medium used by VCS for the insulation of hydrogen storage tanks is for low-temperature gaseous hydrogen, which not only has strong thermal insulation performance but also has no additional energy loss. Rigid Polyurethane Foam (RPF) is a popular thermal insulation material that provides excellent thermal insulation while also being cost-effective [21]. RPF has been used for LNG transportation [22].

In this context, this research is to investigate the effectiveness of applying RPF and VCS for a hydrogen storage system by conducting the design of a large type-C tank for ship liquid hydrogen transportation and storage. Rigid Polyurethane Foam (RPF), Self-evaporation Vapor-Cooled Shield (SVCS), Forced-evaporation Vapor-Cooled Shield with cryogenic hydrogen gas (FVCS+ GH_2) and Forced-evaporation Vapor-Cooled Shield with liquid hydrogen (FVCS+ LH_2) were used to create four insulation schemes. Thermodynamic models were developed and validated. The insulation layer's thermodynamic analysis was performed to investigate the effect of VCS positions on the insulation layer's heat transfer. Finally, research outcomes suggested two optimal design schemes, respectively, for reducing the thickness of the insulation when the heat transfer rate was fixed and reducing the heat transfer rate when the thickness of the insulation was fixed.

1.2 Objective and Scope of Research

How to realize the transportation of liquid hydrogen by ship is a key research direction today. However, some characteristics of liquid hydrogen itself, such as hydrogen embrittlement, strong permeability, and ultra-low storage temperature, make the transportation cost of liquid hydrogen very high. Therefore, finding ways to transport liquid hydrogen efficiently and reduce the transportation cost is an urgent problem that needs to be solved. The world's first hydrogen carrier began operating in Japan and Australia in 2021, but it can only transport 2,500 m^3 of liquid hydrogen at a time and has not realized the large-scale transportation of liquid hydrogen. Therefore, the objectives of this thesis are as follows:

1. Design a large-scale metal tank for liquid hydrogen transportation by shipping: choose a suitable metal material that can achieve low hydrogen embrittlement, low permeability, and low-temperature resistance; design of the thickness of the tank hull while meeting the safety of the cargo.
2. Design the insulation systems of the liquid hydrogen transport tank and study of their heat transfer effect by building thermodynamic models.
3. Optimize the insulation systems on the basis of the insulation designs.

1.3 Outline of the Thesis

The primary objective of the thesis is to design a type-C tank to transport liquid hydrogen efficiently by shipping. To achieve this goal, it is crucial to have a clear understanding of the fundamental properties of liquid hydrogen. Once this is established, a suitable metallic material must be carefully selected as metal shells, and their appropriate thickness must be determined. Following this, insulating layers with high thermal insulation capacity will be designed and evaluated using a thermodynamic model. Lastly, based on the designs, solutions for optimizing the insulating layer will be proposed. This thesis is structured in the following chapters and a brief outline of the content of each chapter is as follows:

1. Chapter 1 (Introduction) This chapter focuses on the background and objectives of the thesis and describes the entire thesis research process.
2. Chapter 2 (Literature Review) This chapter describes the status of hydrogen production, storage and transportation, and explains the Vapor-cooled shield (VCS) system.
3. Chapter 3 (Design of Type-C Tank) This chapter describes the dimensions of the type-C tank and selects AISI type 316L stainless steel as the primary material for the metal shell; calculates the thickness of the tank; and selects the material and thickness of the secondary shell.
4. Chapter 4 (Design of Tank Insulation Layer) This chapter first describes the structure of the insulation layer, and then presents the four designed insulation schemes. Next, thermodynamic models are established for each insulation scheme, and finally, the validity of the thermodynamic models is verified.

5. Chapter 5 (Calculation Results and Discussion) This chapter analyses the calculation results of the thermodynamic models, and then designs two optimization schemes based on these results.
6. Chapter 6 (Conclusions) This chapter summarizes the research contents and findings of the thesis and recommends the next research directions.

1.4 Innovation and Contribution

As environmental pollution continues to get worsen, the utilization of hydrogen energy, which emits no greenhouse gases or sulphides, is considered one of the most crucial clean energy sources for the future. However, liquid hydrogen also has properties such as low temperature (20 K) and hydrogen embrittlement. Enabling a large-scale and long-distance transportation of hydrogen energy is essential for the development of this resource, and ships have immense potential in transporting liquid hydrogen.

Therefore, the main contributions of this thesis are to study of realizing the large-scale transportation of liquid hydrogen by ships as follows:

1. Redesign of the tank on the basis of the large liquid hydrogen carrier MV JAMILA: selection of a more suitable tank metal material, stainless steel type AISI 316L, which has excellent properties in terms of low temperature resistance, resistance to hydrogen embrittlement and resistance to hydrogen permeation; reduction of the thickness of the tank shell while meeting the requirements for safe transport.
2. For the first time, VCS was applied to the design of a large liquid hydrogen transport tank. And the insulation performances of the four insulation designs were studied by building thermodynamic models.
3. Based on the results of the study, two optimization schemes were designed that could reduce the thermal intrusion of liquid hydrogen and the thickness of the insulation layer respectively.

2 Literature Review

2.1 Production of Hydrogen

The element hydrogen is the most widely distributed and abundant element in the universe. Not only is hydrogen the lightest gas, but it is also the cleanest gas for environment. When hydrogen reacts with oxygen, it produces water, and the combustion process releases a huge amount of energy without producing greenhouse gases. Due to its environmental friendliness and high calorific value, hydrogen has been considered the most promising renewable energy source for the future. Various methods have been developed to produce hydrogen from renewable or non-renewable sources.

Steam Methane Reforming (SMR) is the most common method used for large-scale hydrogen production, accounting for approximately 96% of the world's hydrogen production [2, 23]. However, SMR requires fossil fuels, and therefore emits CO_2, which is a major contributor to global warming. Carbon capture and storage can mitigate CO_2 emissions but it comes with additional costs. Another disadvantage of SMR is that it requires a significant amount of water. In addition, scientists are working to reduce the environmental pollution and energy consumption associated with hydrogen formation, such as through the use of dry reforming of methane [24, 25]. This process converts carbon dioxide and methane into carbon monoxide and hydrogen, making it a more sustainable method of hydrogen production.

Alternative methods for hydrogen production include electrolysis, biomass gasification, and thermochemical water splitting [26]. Water electrolysis produces hydrogen in four main ways: alkaline, polymer electrolyte membrane, solid oxide and membraneless electrolysis [27]. Electrolysis uses electricity to split water into hydrogen and oxygen, it can be powered by renewable energy sources such as wind and solar power. Biomass gasification involves the gasification of organic materials such as wood chips or agricultural waste to produce a gas that can be converted into hydrogen. Thermochemical water splitting involves the use of high-temperature heat to split water into hydrogen and oxygen, which can be achieved using concentrated solar energy or nuclear reactors.

Each hydrogen production method has its advantages and disadvantages. SMR is relatively inexpensive and widely used but produces greenhouse gases. Electrolysis can be powered by renewable energy and produces zero emissions, but it is currently more expensive than SMR. Expressed in U.S. dollars, the price of hydrogen from natural gas could be as low as $0.91-1.69/kg, while renewable hydrogen from wind energy could cost as much as $3.56-9.08/kg and $3.34-17.30/kg from solar energy, in 2016 [28]. Biomass gasification is renewable and produces no net carbon emissions but has limited availability of biomass feedstocks. Thermochemical water splitting can be powered by renewable energy and produce no emissions but is currently expensive and requires high-temperature heat sources.

The potential for widely use of hydrogen as an energy carrier is heavily dependent on the scalability and cost-effectiveness of hydrogen production methods. SMR, despite its drawbacks, is currently the most cost-effective method for large-scale hydrogen production,

but there is a growing interest in developing alternative methods that can produce hydrogen more sustainably and cost-effectively. Electrolysis, biomass gasification, and thermochemical water splitting are all promising alternatives but require further research and development to improve their efficiency and reduce costs.

In conclusion, hydrogen production is a critical component of the transition to a low-carbon economy. The current dominant method for hydrogen production, SMR, is inexpensive but emits greenhouse gases, and alternative methods such as electrolysis, biomass gasification, and thermochemical water splitting are promising but require further research and development to become cost competitive with SMR. The choice of hydrogen production method will depend on various factors such as availability of resources, scalability, cost, and environmental impact.

2.2 Status of Hydrogen Storage and Transportation

Hydrogen has great potential as a clean and sustainable energy carrier, but its transportation and storage remain significant challenges. In this part, the current state of knowledge on hydrogen transportation and storage methods, their advantages and disadvantages, and their potential for widely use are summarized.

2.2.1 Hydrogen Transportation

There are currently three main methods of hydrogen transportation: compressed hydrogen gas, liquid hydrogen, and hydrogen carriers. Compressed hydrogen gas is the most commonly used method, which involves compressing hydrogen gas to a high pressure (from 10 to 70 MPa) for transport in specialized containers. Compressed hydrogen storage technology is mainly used in land-based vehicles and aviation, with the size of small hydrogen tanks usually ranging from 0.1 to 20 m^3 [29]. Gaseous hydrogen will be liquefied under the conditions of a standard atmospheric pressure and -253 °C, so there is a huge temperature difference between liquid hydrogen and ambient temperature (about 280 K), resulting in inevitable heat leakage and evaporation [30]. Moreover, liquid hydrogen has a density of 70.8 kg/m^3, which is roughly 800 times greater than the density of gaseous hydrogen under atmospheric conditions [2].

Hydrogen carriers are a developing technology that involves using materials such as metal hydrides or chemical compounds to store and transport hydrogen. Ammonia is also a hydrogen carrier. The conversion between ammonia and hydrogen can be achieved through

the Haber-Bosch reaction [31]. Another important method is the Liquid Organic Hydrogen Carrier (LOHC), which is a liquid or low melting point solid consisting of homocyclic or heterocyclic aromatic rings that can be reversibly hydrogenated and dehydrogenated in the presence of high-temperature environments and catalysts [32]. Hydrogen storage in solid materials has also been extensively studied. These materials can be metallic structures that work like hydrogen sponges, or they can be powders that release hydrogen upon contact with water or increased temperatures [33, 34].

Each hydrogen transportation method has its advantages and disadvantages. Compressed hydrogen gas is a mature technology, and the infrastructure for its transport is relatively well-developed. However, it requires high pressures, which can be a safety concern. The low energy density of compressed gas makes it less efficient for long-distance transport. Liquid hydrogen has a higher energy density than compressed gas, but it requires even more specialized infrastructure and can be challenging to store and transport due to its extremely low temperature. Hydrogen carriers have the potential to be more energy dense than compressed gas or liquid hydrogen, but they are still in the early stages of development and have not yet been widely commercialized.

In the future, the modes and capacities of hydrogen transportation will vary depending on distance and hydrogen demand. For facilities with lower hydrogen demand and shorter transport distances, compressed hydrogen gas is more economically favorable, such as for small-scale power plants. Gaseous hydrogen, which does not require liquefaction, is also cost-effective [62, 63]. Furthermore, lightweight hydrogen storage tanks capable of

withstanding higher pressures are continuously being developed. For example, hydrogen storage tanks made of carbon fiber composite materials with high-density polyethylene liners can withstand pressures of up to 200 bar [64].

Pipeline hydrogen transportation offers significant cost-effectiveness, with research indicating that within a 100-kilometer distance, pipeline transport is the most economical mode of gas transmission [65]. Pipeline transportation of hydrogen is not only safer and more reliable than other transportation methods but also has lower maintenance and operational costs. However, pipeline transportation is affected by the substantial upfront costs required for installation. Additionally, due to hydrogen's inherent permeability, it can lead to significant losses during pipeline transportation. Operating pressures of 10-20 bar inside the pipes can also exacerbate pipeline embrittlement.

Due to variations in natural conditions and research infrastructure, the production costs of green hydrogen differ among countries. Therefore, for countries with high production costs of green hydrogen, importing hydrogen from overseas becomes a more economical choice [66]. For distances exceeding 2500 kilometers, shipping liquefied hydrogen offers a clear economic advantage over pipeline transport [65]. Therefore, the development of vessels designed for liquid hydrogen transport is imperative. On May 6, 2021, KHI obtained preliminary approval (AiP) from NK Class for the design of an LH2 vessel with a cargo capacity of 160,000 m^3 (approximately 12,700 tonnes), which efficiently utilizes evaporated gas to power the vessel. As research progresses, more liquefied hydrogen transport vessels are in the design phase.

2.2.2 Hydrogen Storage

Hydrogen storage is another important challenge that must be addressed for the widely application of hydrogen as a fuel. There are two main methods of hydrogen storage, i.e., physical storage, such as compressed gas or liquid hydrogen and chemical storage, such as metal hydrides or chemical compounds. Physical storage is the most common method used today, but it requires high pressures or low temperatures, making it less practical for certain applications. Chemical storage has the potential to offer higher energy densities and safer storage, but it is still in the early stages of development.

Pipeline is normally used for the transfer of liquid hydrogen and is now also used for storage. It holds great promise because it is not only compact, but can also withstand pressures of up to 100 bar [35]. Several pipeline hydrogen storage projects have been identified and are currently being implemented [36, 37]. However, as the hydrogen storage time increases, hydrogen embrittlement can cause severe damage to the pipe materials - metal, leading to cracking or even fracture of the pipeline systems [38].

Underground hydrogen storage is an effective way to store large quantities of hydrogen in a medium and long term. It is similar to the underground storage of natural gas, which has been widely used by oil companies for hundreds of years [39]. The use of insulated cryogenic vessels is an effective way to prevent hydrogen from evaporation [40]. Most liquid hydrogen tanks are spherical, as spherical tanks have the smallest heat transfer surface area per unit volume [41]. Cylindrical tanks are sometimes used because they are

easier and cheaper to manufacture than spherical tanks, and their volume-to-surface area ratio is nearly the same [42].

NASA built two large cryogenic storage tanks for its space shuttle in 1965, which can hold 3,200 m^3 of liquid hydrogen. These tanks are still one of the world's largest cryogenic hydrogen storage tanks [43]. In 2018, NASA started construction of an additional storage tank at Launch Complex 39B, which provides an additional storage capacity of 4,732 m^3 [12].

The potential for widely use of hydrogen as an energy carrier is heavily dependent on the scalability and cost-effectiveness of hydrogen transportation and storage methods. Compressed hydrogen gas is currently the most widely used method of hydrogen transport, but its low energy density and high-pressure requirements limit its practicality for some applications. Liquid hydrogen and hydrogen carriers offer the potential for higher energy densities, but still require significant infrastructure development and face technical challenges. Hydrogen storage, especially chemical storage, also requires further research and development to improve its efficiency and reduce costs.

In conclusion, hydrogen transportation and storage are critical components of the transition to a low-carbon economy. The current dominant method of hydrogen transportation, compressed gas, is mature but has limitations, and alternative methods such as liquid hydrogen and hydrogen carriers are still in the early stages of development. Hydrogen storage also requires further research and development to become more practical and cost-

effective. The choice of hydrogen transportation and storage method will depend on various factors such as availability of resources, scalability, cost, and environmental impact.

2.2.3 Sensible heat and latent heat of vaporisation of hydrogen at different pressures

Hydrogen is a clear and sustainable fuel that has gained increasing attention in recent years due to its potential to replace fossil fuels. Latent heat is energy released or absorbed, by a body or a thermodynamic system, during a constant-temperature process. At 0.1 MPa and a temperature of 20 K, the vaporization heat of hydrogen is approximately 4.49×105 J/kg [10]. This means that a significant amount of energy is required to convert hydrogen from a liquid to a gas. Sensible heat, on the other hand, refers to the amount of energy required to raise the temperature of a substance without changing its phase. In the case of hydrogen, its sensible heat is relatively low due to its low specific heat capacity. The specific heat capacity of hydrogen is approximately 14.3 J/g·K, which is much lower than other common gases such as nitrogen and oxygen.

It is crucial to understand how sensible heat is utilized for liquid hydrogen storage. As the pressure of liquid hydrogen storage increases, the proportion of sensible heat in the total cold energy becomes higher, and the potential effect of VCS becomes more significant [10]. Therefore, this thesis sets the tank pressure to 0.4 MPa to increase the sensible heat ratio without significantly increasing the tank wall pressure. The core objective of VCS is to recover sensible heat from cryogenic hydrogen and cool the neighbouring RPF. For this purpose, the cryogenic hydrogen gas must be able to exchange sufficient heat with VCS

heat exchanger tubes, and the in-transit resistance drop of VCS heat exchanger tubes should not be too large. Additionally, it is necessary for the VCS material to have good thermal conductivity and for the thermal resistance between the VCS and the adjacent RPF to be as small as possible.

Hydrogen has a high vaporization heat and a low sensible heat due to its low boiling point and specific heat capacity. These properties have important implications for the performance of hydrogen fuel cells and other hydrogen-based technologies. As research in this area continues, it is likely that new insights will be gained into the properties of hydrogen and their implications for energy applications.

2.3 Vapor-Cooled Shield (VCS)

Vapor-cooled shields are used in a variety of applications to protect sensitive components from high temperatures. These shields are designed to absorb heat transferred from it surrounding by evaporating liquid coolant. Vapor-cooled shields have been used in a range of applications, including spacecraft and nuclear reactors.

Conventional VCS mainly uses external cooling sources to obtain better insulation performance [18, 19]. The use of vapor-cooled shields in space applications has been extensively studied [44, 45]. The X-ray spectrometer(XRS) and the wide-field infrared detector on the Suzuki satellite are extremely sophisticated detection instruments that need to be provided with a cold environment when the satellite is launched [46]. Therefore, VCSs were designed to protect a spacecraft from high temperatures during re-entry into the Earth's atmosphere. Between the main shell and the neon tank of XRS dewar, there are three VCS: Inner VCS, Middle VCS and Outer VCS, which are cooled by sublimed neon and evaporated helium. These shields reduce incident radiation from the main shell to the neon tank.

VCS has also been studied for use in nuclear reactors. VCS was used to protect the reactor vessel from the high temperatures generated during operation. The shield was made of a thin layer of metal that was cooled by a liquid coolant. The coolant evaporated when it came into contact with the hot metal, carrying away heat and preventing damage to the reactor vessel.

Research has focused on the design of VCS, including the use of channels to improve cooling efficiency. As technology advances, VCS is likely to become even more important in protecting sensitive components from high temperatures. The material, structure and heat transfer effect of VCS still have not yet been fully understood in this field, and further simulation and experimental verification work are needed [47].

3 Design of Type-C Tank

Large liquid hydrogen transport by ships is unquestionably an option for achieving large-scale hydrogen energy transport across continents and regions.

3.1 Tank Design

Type-C tanks are insulated cylindrical, bi-lobe or tri-lobe shaped tanks that can be fully or partially pressurized, depending on the liquefied gas to be stored. The construction is similar to a pressure vessel, based on the cylindrical design for optimal material usage vs. internal pressure. A. N. Alkhaledi et al. [16, 48] designed a large-scale hydrogen transport ship, MV JAMILA, which has four type-C tanks and can carry a total of 280,000 m^3 of liquid hydrogen. However, the ship has aluminium as the metal shell of the liquid hydrogen tanks. Aluminium is soft and deformable and has only 1/5 the tensile strength of mild steel; furthermore, the thickness of the MV JAMILA's metal shell is 434 mm, which is not justified by the ship's design. The high construction costs associated with the use of aluminium as the tank metal shell and the increase in the ship's operating costs due to the excessively heavy tank (87,819 tonnes) will significantly affect the ship's economy. In order to assess the insulation and economy of the tank, the main parameters of the MV JAMILA and the parameters of the tank are quoted. Table 1 displays the main parameters and dimensions of MV JAMILA. Table 2 displays the internal parameters of the liquid hydrogen transport tank of MV JAMILA, which have also been used in the design of this research.

Table 1 Main parameters and dimensions of MV JAMILA.

Ship parameters	Values	Units
Class	JAMILA	–
Vessel type	LH_2 tanker	–
Total displacement	230,000	tonnes
Lightweight (LWT)	208,000	tonnes
Deadweight (DWT)	22,000	tonnes
Length overall (LOA)	370	m
Length between perpendicular (LBP)	367.5	m
Length on water line (LW)	367.9	m
Extreme breadth (B)	75	m
Depth (D)	35	m
Draft (full load condition)	10.012	m
Draft (unload condition)	9.263	m
Block coefficient (full-load condition)	0.819	–
Block coefficient (unloaded condition)	0.813	
Ship speed	18	knot
Liquid hydrogen cargo tank weight (Aluminium)	87,819 (21,955 × 4)	tonnes
Liquid hydrogen cargo tank capacity	282,400 (70,600 × 4)	m^3
Liquid hydrogen cargo weight	20,000 (5,000 × 4)	tonnes

Table 2 Internal parameters of the liquid hydrogen transport tank of MV JAMILA.

Internal tank parameters	Values	Units
Volume	70,600	m^3
Diameter	26.38	m
Cylindrical section length	111.62	m
Head type	Spherical head	
Excess volume	0.252	%
Boil-off rate	0.1	%

3.2 Selection of Metal Shell Material

Properties of metals change as the temperature decreases. The properties of most materials, such as their elastic modulus, tensile strength, and yield strength, increase with decreasing temperature [49]. Liquid hydrogen is stored or transported at a temperature of 20 K in liquid cargo tanks, which imposes extremely stringent requirements for the low-temperature performance of the metal materials selected.

In a hydrogen environment at a low temperature, the hydrogen embrittlement effect on metals is inevitable. The hydrogen enhanced decohesion mechanism (HEDE), adsorption induced dislocation emission (AIDE), and hydrogen enhanced localized plasticity (HELP) are the main mechanisms responsible for the hydrogen embrittlement [50, 51]. The presence of hydrogen reduces the tensile and fatigue strength, while reducing the ductility and making the metal brittle. Due to their low hydrogen embrittlement, austenitic stainless steels have been widely used in the production of hydrogen energy-related equipment [52].

The world's first hydrogen transport ship, Suiso Frontier, uses austenitic stainless steel as its tank material [14]. Austenite in stainless steel is of a face-centred cubic crystal structure with superior plastic deformation ability. As the temperature decreases, the strength of austenitic stainless steel increases, while maintaining excellent plasticity and low-temperature impact resistance [53, 54] which is required for the storage of liquid hydrogen. The 300 series is widely used in low-temperature liquid storage and transportation containers. A among which 304, 304L, 316, 316L, 321, 347 and so on are used [53, 55].

In the ocean environment where ships operate, corrosion-resistant materials are more advantageous. For example, adding Mo to 316L stainless steel improves its resistance to chloride ion corrosion, making it suitable for ocean environments with high salt spray concentrations [54]. For this reason, this thesis has selected AISI type 316L stainless steel as the main material for the metal shell and an annealing process is used to eliminate excess stress. Table 3 shows the specific parameters of AISI type 316L stainless steel [56].

Table 3 AISI type 316L stainless steel (annealed plate) related parameters.

Parameter names	Values	Units
Density	8,000	kg/m^3
Hardness, Brinell	146	N/mm^2
Tensile Strength, Ultimate	560	MPa
Tensile Strength, Yield	235	MPa
Elongation at Break	55	%
Modulus of Elasticity	193	GPa
Charpy Impact	103	J

3.3 Calculation of Metal Shell Thickness

For tanks with certain internal pressure, a reasonable and rigorous design of the tank wall thickness can ensure the safety of the liquid cargo without leaks, while also controlling the weight of the tank and keeping the economy in mind.

The relevant dimensions of the C-type tank designed in this study can be viewed in Table 2. The wall thickness of Type-C tanks used for transporting cryogenic liquid cargoes can be calculated according to the specifications of the China Classification Society (CCS) and should meet with the following requirements [57].

For the thickness of the cylindrical shell plate,

$$t \geq \frac{p_{eq} D_i}{2\sigma_m \phi - p_{eq}} + C \quad (1)$$

where t is the thickness of shell, mm; p_{eq} is the internal pressure of the tank, take 0.45 MPa; D_i is the inside diameter of the tank, 26,380 mm; σ_m is the allowable membrane stress, take 131.25 N/mm^2; C is the corrosion addition, mm. Because anti-rust treatment measures will be used on the tank's corrosion-prone areas, the corrosion increment will be ignored; ϕ is the welded joint efficiency facto, take 0.95 here.

The thickness of spherical end plate can be expressed by the following equation,

$$t \geq \frac{p_{eq} D_i y}{2\sigma_m \phi - 0.5 p_{eq}} + C \quad (2)$$

where, y is the shape factor, generally to be taken as 0.55 for a spherical end.

In addition to meeting the above conditions, the thickness of plates in any area is not to be less than:

$$t_{\min}=3+\frac{D_{\mathrm{i}}}{1500} \tag{3}$$

Finally, the thickness of the primary shell is calculated to be 47.7 mm.

3.4 The Secondary Shell

In general, the IGC Code (International Code for the Construction, 1986) requires the installation of an independent secondary shell for liquid cargo tanks with a cargo temperature of 218 K (-55 °C) under atmospheric pressure [58]. Additionally, in the event that the liquid-tight primary shell is damaged and the liquid cargo leaks, the secondary shell must contain the cryogenic liquid cargo for 15 days. Thus, for liquid hydrogen transported at 20 K (-253 °C), this research designs the secondary shell using the same AISI Type 316L stainless steel as the main shell and with a thickness that is consistent with that of the primary shell.

4 Design of Tank Insulation Layer

4.1 Physical Model of Insulation Layer Structure

The liquid hydrogen transportation tank consists of two layers of shells and a layer of insulation. Insulation is formed by a combination of VCS and RPF that is installed between the metal primary and secondary shells. Figure 1 depicts a sketch of the liquid hydrogen transport tank under design. T_{in} and T_{out} are the inlet and outlet hydrogen temperatures of the VCS heat exchanger tubes; r_{R1} and r_{R2} are the radii of the cryogenic and hot boundaries of the insulation from the axis of the longitudinal axis of the tank； r_{VCS} is the radii of the VCS heat exchanger tube in the insulation from the axis of the longitudinal axis of the tank; T_1 and T_2 are the surface temperatures of the cryogenic and hot boundaries of the insulation; T_{VCS} is the temperature of the wall of the VCS heat exchanger tube; T_∞ is the temperature of the air surrounding the tank, 318 K;

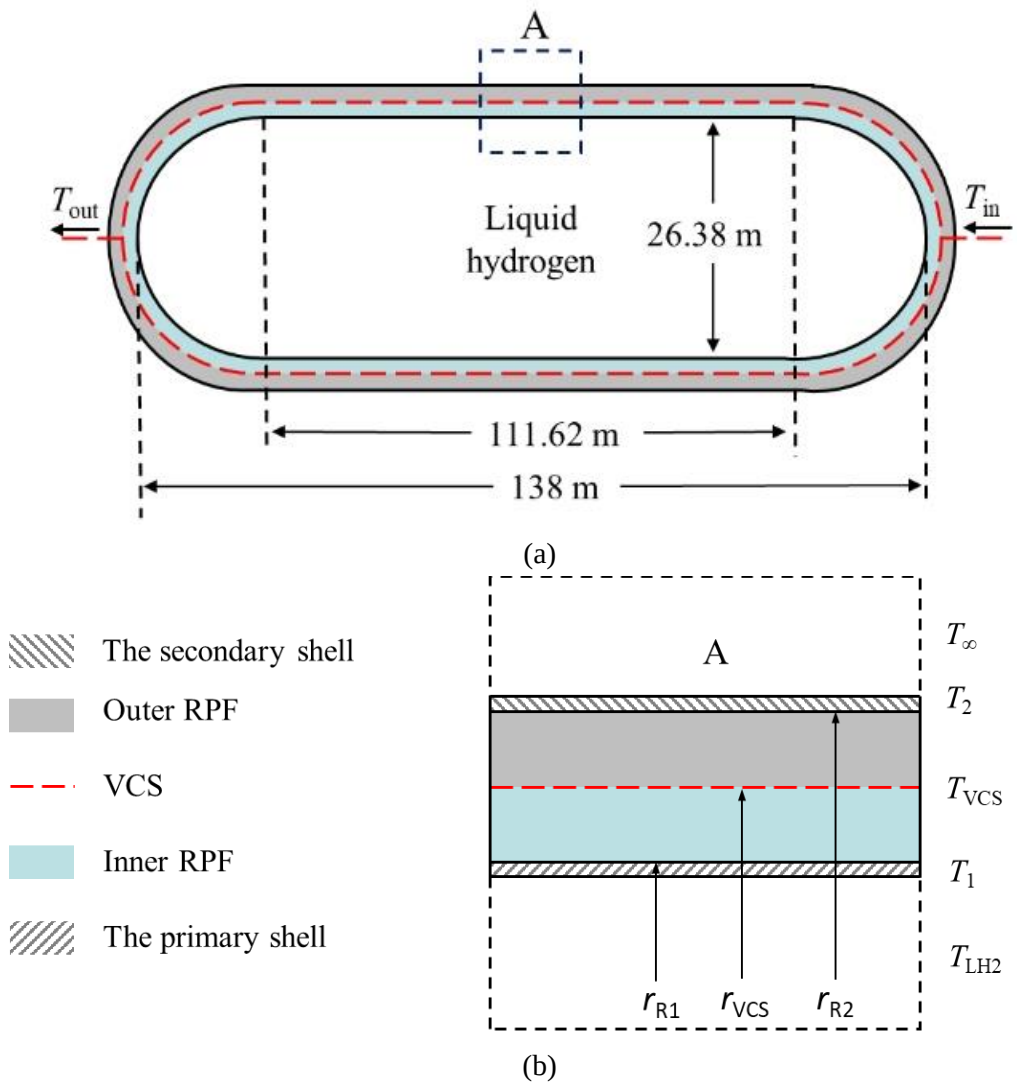

Figure 1 The sketch of the liquid hydrogen transport tank under design.

The material of the VCS heat exchanger tubes needs to have good thermal conductivity and low temperature resistance. The VCS in this research is composed of AISI 316L Stainless Steel heat exchanger tubes with dimensions of Φ9.525 mm × 1.245 mm. The heat exchanger tubes are spaced about 50 mm apart and arranged symmetrically around the longitudinal axis of the tank, with a total of 1,460 heat exchanger tubes. All the tubes will form an insulating layer to reduce heat transfer from the outer RPF. Figure 2 depicts the schematic of how the VCS heat exchanger tubes are laid. The low-temperature hydrogen

gas is through the long and thin tubes, which is approximated as a straight tube because the bending radius of the tube is much larger than the tube diameter.

The design of the insulation layer for the liquid hydrogen transport tank is crucial, as it directly impacts the amount of heat transfer and evaporation of the liquid hydrogen. To reduce the amount of heat leakage and prevent excessive evaporation of the liquid hydrogen inside the tank, this thesis investigated four design schemes for the insulation layer structure of the tank: Single Rigid Polyurethane Foams, Self-evaporation Vapor-Cooled Shield and Rigid Polyurethane Foams, Forced-evaporation Vapor-Cooled Shield with cryogenic hydrogen gas and Rigid Polyurethane Foams, Forced-evaporation Vapor-Cooled Shield with liquid hydrogen and Rigid Polyurethane Foams.

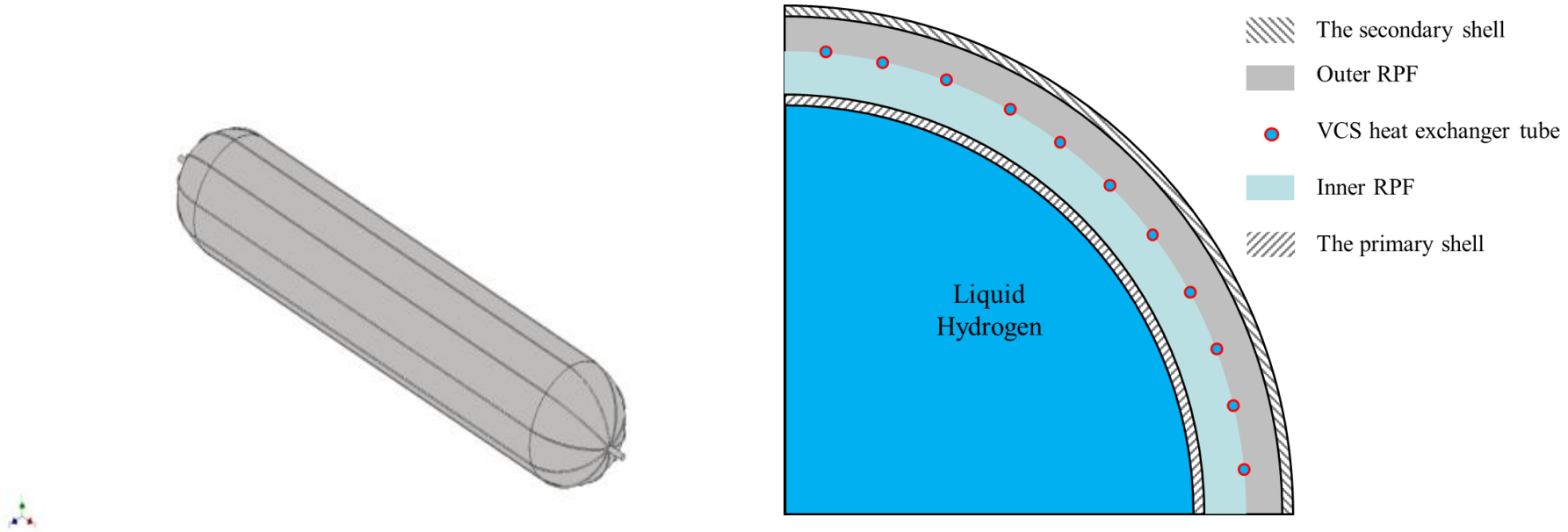

Figure 2 Schematic diagram of how the VCS heat exchanger tubes is laid.

4.2 Assumption of Conditions

This research discusses the steady-state heat exchange between the liquid hydrogen transport tank and the tank surrounding, where the evaporation of liquid hydrogen and the temperature distribution of the insulation remain constant. The following conditions are assumed:

(1) The environment around the tank is assumed to be an air temperature of 318 K and a pressure of 0.1 MPa. [57].

(2) The temperature of the liquid hydrogen in the liquid hydrogen transport tank is 20 K, and its pressure is 0.4 MPa [14]. The temperature of the primary shell is the same as that of the liquid hydrogen; the temperature of the secondary shell is the same as that of the outermost surface of tank.

(3) The VCS heat exchanger tubes are embedded in the RPF and in a close contact with it, the temperature of the wall of the VCS heat exchanger tube and the temperature of the RPF in contact with it are equal.

(4) All heat transferred into the liquid hydrogen transport inside the tank would contribute to boil-off gas production.

(5) Both the primary and secondary shells are constructed using AISI type 316L stainless steel with high thermal conductivity, resulting in negligible thermal insulation performance.

4.3 Single Rigid Polyurethane Foams

In this part, the insulation layer is filled with RPF. The primary method of heat transfer in the insulation layer is solid heat conduction, as shown in Figure 3. Q_{total} is the heat transferred from the tank surrounding to the tank's outermost layer; Q_1 is the heat transfer through the RPF layer; Q_0 is the heat transfer that ingresses the liquid hydrogen inside the tank.

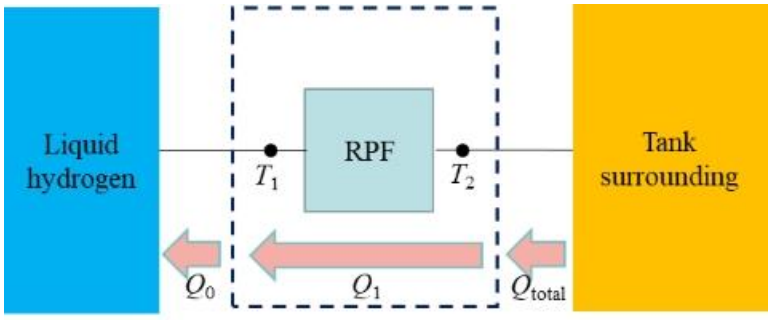

Figure 3 Schematic diagram of heat transfer process with single RPF.

The relevant thermodynamic model can be constructed based on the heat transfer schematic diagram.

The heat transfer between the tank surrounding and the tank's outermost layer (the secondary shell) primarily takes place through radiation and convective of heat transfer [59].

$$Q_{\text{total}} = Q_{\text{rad}} + Q_{\text{con}} \tag{4}$$

Q_{total} is the heat transferred from the tank surrounding to the tank′s outermost layer; Q_{rad} is the radiative heat transferred that occurs between the tank outermost surface and the tank surrounding; Q_{con} is the convective heat transfer from the tank surrounding.

$$Q_{\text{rad}} = \varepsilon\delta(A_{\text{c}} + A_{\text{s}})(T_{\infty}^4 - T_2^4) \tag{5}$$

in which ε is the emissivity (with a value ranging from 0 to 1). The outermost surface of the tank is protected by an aluminium-plated protective layer, and the emissivity of aluminium is 0.03; δ is the Stefan Boltzmann constant, 5.675×10^{-8} W/m^2·K^4; A_{c} and A_{s} are the areas of the secondary shell's long cylindrical outer surface and spherical outer surface, respectively, m^2; T_{∞} is the temperature of the air surrounding the tank, 318 K; T_2 is the temperature of the outermost surface of the tank, K.

$$Q_{\text{con}} = h_{\text{c}}A_{\text{c}}(T_{\infty} - T_2) + h_{\text{s}}A_{\text{s}}(T_{\infty} - T_2) \tag{6}$$

where h_{c} and h_{s} are the convective heat transfer coefficients of the outmost surface of the long cylinder and spherical outer surface, W/m^2·K.

$$h_{\text{c}} = \frac{Nu_{\text{c}}\lambda_{\infty}}{D_{\text{c}}} \tag{7}$$

$$h_{\text{s}} = \frac{Nu_{\text{s}}\lambda_{\infty}}{D_{\text{s}}} \tag{8}$$

in which Nu_c and Nu_s are the Nusselt numbers of the long cylindrical outer surface and spherical outer surface; D_c and D_s are the feature sizes of the long cylindrical outer surface and spherical outer surface, m; λ_∞ is the thermal conductivity of air, at a standard atmospheric pressure and 318 K, take 0.028 W/m·K.

Based on heat transfer theory [59], it is recommended that the Nussle number of the outer surface of a long cylinder be calculated using the following relation,

$$Nu_c = \left\{ 0.60 + \frac{0.387 Ra_c^{\frac{1}{6}}}{\left[1 + \left(\frac{0.559}{Pr_\infty}\right)^{\frac{9}{16}}\right]^{\frac{8}{27}}} \right\}^2 \tag{9}$$

Where, Ra_c is the air's Rayleigh number on the outer surface of a long cylinder; Pr_∞ is the air's Prandtl number in tank surrounding.

$$Ra_c = \frac{g\beta_\infty D_c^3 (T_\infty - T_2)}{\alpha_\infty \nu_\infty} \tag{10}$$

Where, g is the acceleration of gravity, 9.8 m/s^2; β_∞ is the volumetric expansion coefficient of air, $\beta_\infty = \frac{1}{T_\infty(K)}$; ν_∞ is the kinematic viscosity of air, and at a standard atmospheric pressure and 318 K, take 1.77×10^{-5} m^2/s; α_∞ is the thermal diffusivity of air, take 2.51×10^{-5} m^2/s.

$$Pr_{\infty} = \frac{\nu_{\infty}}{\alpha_{\infty}} \tag{11}$$

$$\alpha_{\infty} = \frac{\lambda_{\infty}}{\rho_{\infty} c_{\infty}} \tag{12}$$

Where, c_{∞} is the specific heat of air, take 1,007.41 J/kg·K; ρ_{∞} is the air density, take 1.10 kg/m^3.

Nusselt number on the outer surface of a sphere [59],

$$Nu_{\mathrm{s}} = 2 + \frac{0.589 Ra_{\mathrm{s}}^{\frac{1}{6}}}{\left[1 + \left(\frac{0.469}{Pr_{\infty}}\right)^{\frac{9}{16}}\right]^{\frac{4}{9}}} \tag{13}$$

Ra_{s} is the air's Rayleigh number on the outer surface of a sphere,

$$Ra_{\mathrm{s}} = \frac{g \beta_{\infty} D_{\mathrm{s}}^3 (T_{\infty} - T_2)}{\alpha_{\infty} \nu_{\infty}} \tag{14}$$

In the case of a single RPF, heat is transferred from the tank surrounding passes through the RPF layer and eventually to the liquid hydrogen inside the tank. The formula for this process can be expressed by using the energy conservation law,

$$Q_{\mathrm{total}} = Q_1 = Q_0 \tag{15}$$

To ensure economy, this research requires that the boil-off rate of liquid hydrogen does not exceed 0.1% of the total mass of liquid hydrogen per day in the tank [16]. Therefore, the heat ingressing the liquid hydrogen tank is required:

$$Q_0 \leq \frac{M * Q_{\mathrm{v}}}{h} \tag{16}$$

Where, M is the maximum mass allowed to evaporate per tank per day, 5,000 kg; Q_{v} is the latent heat of vaporization of liquid hydrogen evaporation at 0.4 MPa, 20 K, take 4.49×10^5 J/kg; h is the time, s.

Heat conduction is the primary way of heat transfer through the RPF; convective and radiant heats are negligible.

$$Q_1 = Q_{\mathrm{c}} + Q_{\mathrm{s}} \tag{17}$$

Where, Q_{c} is the heat conduction of the hollow long cylinder of the RPF, W; Q_{s} is the heat conduction of spherical shell of the RPF, W.

$$Q_{\mathrm{c}} = \frac{2\pi l_{\mathrm{R}} \lambda_{\mathrm{R}} (T_2 - T_1)}{\ln\left(\frac{r_{\mathrm{R2}}}{r_{\mathrm{R1}}}\right)} \tag{18}$$

where T_1 and T_2 are the surface temperatures on the two sides of the RPF, T_1 takes 20 K; r_{R1} and r_{R2} are the radii of the two sides of the RPF, r_{R1} takes 13.24 m; l_{R} is the length of

the RPF hollow long cylinder, take 111.62 m; λ_{R} is the thermal conductivity of RPF, take 0.013 W/m·K.

$$Q_s = \frac{4\pi\lambda_{\mathrm{R}}(T_2 - T_1)}{\left(\frac{1}{r_{\mathrm{R1}}}\right) - \left(\frac{1}{r_{\mathrm{R2}}}\right)} \tag{19}$$

According to the Eqs. (1), (12), (13), (14) the value of r_{R2} can be calculated, and the difference between r_{R2} and r_{R1} is the thickness of the RPF. Ultimately, the thickness of the insulation of the single RPF is calculated to be 1.84 m.

4.4 Self-evaporation Vapor-Cooled Shield and Rigid Polyurethane Foams

In this part, the heat transfer from the external environment causes the liquid hydrogen in the liquid hydrogen tank to self-evaporate. This evaporated cryogenic hydrogen gas is then fed into the VCS heat exchanger tubes to cool the insulation and reduce the heat transfer.

As shown in Figure 4, the heat transfer, Q_2, from the surroundings of the tank first passes through the Outer RPF by solid heat conduction. Q_2 is divided into two parts: one part of the heat transfer, Q_{GVCS}, it is absorbed by the cryogenic hydrogen gas in the SVCS heat exchanger tubes. While the other part, Q_1, goes to the Inner RPF. Q_1 passes through the Inner RPF by solid heat conduction. The low-temperature hydrogen gas is evaporated from the liquid hydrogen due to the heat transfer Q_0.

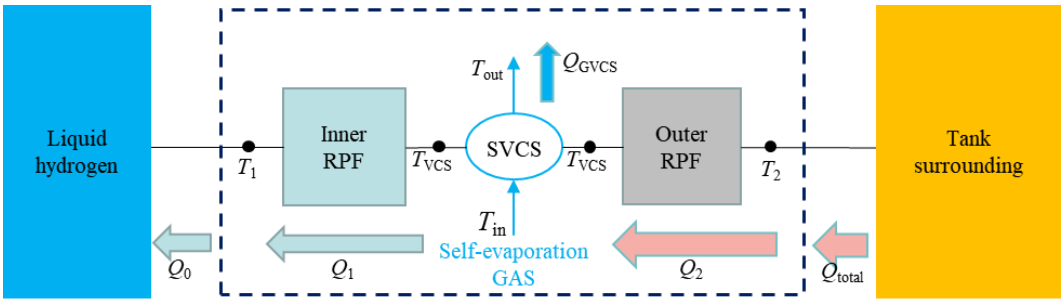

Figure 4 Schematic diagram of the heat transfer process of the insulation layer composed of SVCS and RPF.

For the insulation layer composed of Self-evaporation Vapor-Cooled Shield (SVCS) and RPF, heat transfer from the tank surrounding first passes through the outer RPF layer.

When the heat transfer passes through the wall of the VCS heat exchanger tubes, the low-temperature hydrogen gas in inside the tubes absorbs some of the heat transferred. The remaining heat ingress enters to the liquid hydrogen after passing through the inner RPF layer and eventually leading to evaporation of the liquid hydrogen. The cryogenic hydrogen gas formed by the evaporation of liquid hydrogen will then fed into the VCS heat exchanger tubes.

In insulated systems installed with VCS, steady state heat transfer is marked by the outlet temperature of the VCS heat exchanger tube T_{out} being the same as the wall temperature of the heat exchanger tube T_{VCS}. Once the temperature of the hydrogen in the VCS heat exchanger tube reaches the wall temperature, the hydrogen in the tube is no longer convectively heat exchanged.

The heat transfer from the outside of the tank can be calculated from Eqs. (1) to Eqs. (11). The heat transfer within the tank insulation can be calculated by the following equation:

$$Q_0 = Q_1 \tag{20}$$

$$Q_{\text{total}} = Q_2 \tag{21}$$

$$Q_2 = Q_1 + Q_{\text{GVCS}} \tag{22}$$

The calculation of Q_2 and Q_1 are the same as Eqs. (14), (15), and (16).

Heat exchanger rate to hydrogen inside the VCS is:

$$Q_{\mathrm{GVCS}} = 1460 h_{\mathrm{GH2}} A_{\mathrm{GVCS}} (T_{\mathrm{GVCS}} - \bar{T}_{\mathrm{GH2}}) \quad (23)$$

Where, 1,460 is the number of VCS heat exchanger tubes installed in each tank; h_{GH2} is the convective heat transfer coefficient between the low-temperature gas hydrogen in the VCS heat exchanger tube and the tube wall, W/m^2·K; A_{GVCS} is the heat transfer area of the inner wall of the heat exchanger tube from the start of heat transfer between the hydrogen gas and the tube wall until steady state heat transfer is achieved, m^2; T_{GVCS} is the tube wall temperature, K; $\bar{T}_{\mathrm{GH2}}$ is the feature temperature of hydrogen gas in the tube, K, $\bar{T}_{\mathrm{GH2}} = \frac{T_{\mathrm{out}} - T_{\mathrm{in}}}{2}$.

$$h_{\mathrm{GH2}} = \frac{\lambda_{\mathrm{GH2}} Nu_{\mathrm{GH2}}}{D_{\mathrm{VCS}}} \quad (24)$$

D_{VCS} is the diameter of VCS heat exchanger tube, take 0.007 m; λ_{GH2} is the thermal conductivity of hydrogen gas, W/m·K; Nu_{GH2} is the Nusselt number of the inner wall of the heat exchanger tube.

The Gnielinski correlation is suitable for forced convection, including transition areas with Reynolds numbers over 3,000 [59],

$$Nu_{\mathrm{GH2}} = \frac{\left(\frac{f}{8}\right)(Re_{\mathrm{GH2}} - 1000)Pr_{\mathrm{GH2}}}{1 + 12.7\left(\frac{f}{8}\right)^{\frac{1}{2}}\left(Pr_{\mathrm{GH2}}^{\frac{2}{3}} - 1\right)} \tag{25}$$

where Pr_{GH2} is the Prandtl number of hydrogen gas in VCS heat exchanger tube; f is the friction factor between the hydrogen gas and the wall of the heat exchanger tube [59],

$$f = (0.790 \ln Re_{\mathrm{GH2}} - 1.64)^{-2} \tag{26}$$

Reynolds number Re_{GH2} can be calculated by the following formula,

$$Re_{\mathrm{GH2}} = \frac{\rho_{\mathrm{GH2}} v_{\mathrm{GH2}} D_{\mathrm{VCS}}}{\mu_{\mathrm{GH2}}} \tag{27}$$

$$v_{\mathrm{GH2}} = \frac{\dot{m}}{1460 \rho_{\mathrm{GH2}} A_{\mathrm{GH2}}} \tag{28}$$

where ρ_{GH2} is the density of low-temperature hydrogen gas in the VCS, kg/m^3; μ_{GH2} is the dynamic viscosity of the hydrogen gas in the VCS, Pa·s; v_{GH2} is the average velocity of the hydrogen gas in the VCS, m/s; A_{GH2} is the cross-sectional area of the VCS heat exchanger tube, m^2; $\dot{m}$ is the mass flow rate of low-temperature hydrogen gas evaporated in a cargo tank, kg/s.

According to the law of energy conservation, the heat absorbed by VCS can also be expressed as:

$$Q_{\mathrm{GVCS}} = \dot{m}(H_{\mathrm{Gin}} - H_{\mathrm{Gout}}) \tag{29}$$

in which H_{Gin} and H_{Gout} are the enthalpy of the hydrogen gas at the inlet of the VCS tube and the enthalpy of the hydrogen at outlet of the VCS tube, J/kg.

According to assumption 4, all heat transferred to liquid hydrogen inside tank is consumed for liquid hydrogen evaporation.

$$\dot{m} = \frac{Q_0}{Q_{\mathrm{v}}} \tag{30}$$

The above equations will form a closed thermodynamic model of the insulation of SVCS and RPF. As the installation position of the SVCS within the insulation varies, there will be different heat transfer and heat distribution in insulation.

4.5 Forced-evaporation Vapor-Cooled Shield with cryogenic hydrogen gas and Rigid Polyurethane Foams

In this part, hydrogen will be used as fuel to provide energy for the operation of the ship. The fuel hydrogen is supplied from 4 liquid cargo tanks and there is no separate fuel tank. The liquid hydrogen ship is driven by two MAN B&W 7S70ME-C two-stroke low-speed diesel engines, electronically controlled. The total output of these engines at 91 rpm (Revolutions per minute) is 43. 54 MW. The conversion of the diesel engines to hydrogen engines would require a daily consumption of 54 tonnes of hydrogen at the same total output. During the operation of the ship, a certain amount of liquid hydrogen is extracted to the heat exchanger and forced to evaporate into cryogenic hydrogen gas. This cryogenic hydrogen gas is then fed into the VCS heat exchanger tubes to participate in the tank insulation and is finally delivered to the engine for combustion.

Figure 5 depicts the diagram of the heat transfer process of the insulation layer composed of FVCS with cryogenic hydrogen gas and RPF. The main heat transfer processes are similar to Figure 4, the major difference being the different mass flow rates of the cryogenic hydrogen gas fed into the VCS heat exchanger tubes.

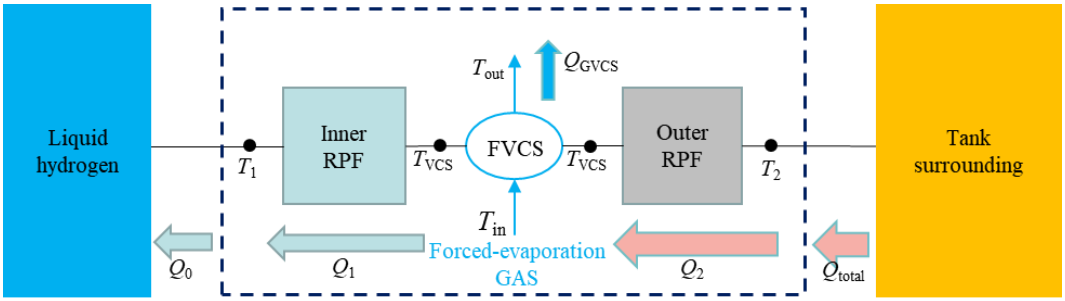

Figure 5 Schematic diagram of the heat transfer process of the insulation layer composed of FVCS with cryogenic hydrogen gas and RPF.

The daily hydrogen consumption of a propulsion system with a total power output of 43.54 MW is 54 tonnes. It means that each hydrogen transport tank's FVCS heat changer tubes need pass 13.51 tonnes of hydrogen per day. Where the hydrogen consumption and the diameter of the FVCS heat exchanger tube are determined, the mass flow rate per heat exchanger tube can be determined,

$$\dot{m}^* = \frac{M^*}{h} \tag{31}$$

where M^* is the mass of hydrogen gas passing through the heat exchanger tube of every tank per day in the case of forced evaporation, 13,510 kg; $\dot{m}^*$ is the mass flow rate of hydrogen gas passing through the heat exchanger tube of every tank per day in the case of forced evaporation, kg/s.

With the FVCS installed, the final calculation of the mass flow rate of cryogenic hydrogen gas to be forcibly evaporated per cargo tank is 0.16 kg/s.

4.6 Forced-evaporation Vapor-Cooled Shield with liquid hydrogen and Rigid Polyurethane Foams

In this research, hydrogen will be used as fuel to power the operation of the ship. A certain amount of liquid hydrogen will be fed directly into the heat exchanger tubes of the VCS, participate in the tank insulation. First the liquid hydrogen will undergo convective heat transfer with the wall of the tube, where it will be gradually heated up in the flow until it evaporates into low temperature hydrogen gas; the low temperature hydrogen gas will continue to participate in the heat transfer in the heat exchanger tube; finally, the hydrogen will be transported to the engine for combustion. It is assumed that there is no gas-liquid mixing in the heat exchanger tube and that the liquid hydrogen is completely vaporized into hydrogen gas at some point in the tube.

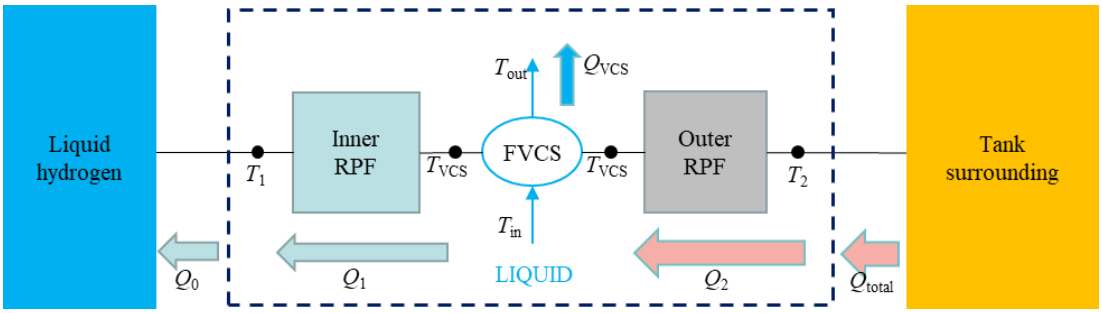

Figure 6 Schematic diagram of the heat transfer process of the insulation layer composed of FVCS with liquid hydrogen and RPF.

When the heat transfer between the tank and the external environment is in a steady state, the heat transfer in the VCS heat exchanger tube consists of two main components, the heat

transfer between the liquid hydrogen Q_{LVCS} and the tube wall and the heat transfer between the cryogenic hydrogen gas and the tube wall Q_{GVCS}:

$$Q_{\mathrm{VCS}} = Q_{\mathrm{LVCS}} + Q_{\mathrm{GVCS}} \tag{32}$$

The heat transfer of liquid hydrogen in the VCS heat exchanger tubes can be calculated using the latent heat of vaporization of liquid hydrogen at 0.1 MPa and 20 K as follows:

$$Q_{\mathrm{LVCS}} = \frac{M^* * Q_{\mathrm{v}}^*}{h} \tag{33}$$

Where, Q_{v}^* is the latent heat of vaporization of liquid hydrogen evaporation at 0.1 MPa, 20 K, take 4.49×10^5J/kg.

Q_{LVCS} can also be calculated using the following formula:

$$Q_{\mathrm{LVCS}} = 1460 h_{\mathrm{LH2}} A_{\mathrm{LVCS}} (T_{\mathrm{LVCS}} - \bar{T}_{\mathrm{LH2}}) \tag{34}$$

Where, h_{LH2} is the convective heat transfer coefficient between the liquid hydrogen in the VCS heat exchanger tube and the tube wall, W/m^2·K; A_{LVCS} is the heat transfer area of the inner wall of the heat exchanger tube from the start of heat transfer between the liquid hydrogen and the tube wall until the liquid hydrogen is evaporated into hydrogen gas, m^2; T_{LVCS} is the tube wall temperature, K; $\bar{T}_{\mathrm{LH2}}$ is the feature temperature of liquid hydrogen in the tube, take 20 K.

Due to the forced laminar flow of liquid hydrogen in the tube, the tube diameter is small and the temperature difference between the fluid and the wall is small. Therefore, the effect of natural convection on the forced flow heat transfer can be ignored and the Sieder and Tate [60] correlation equation can be applied:

$$h_{\mathrm{LH2}} = 1.86\frac{\lambda_{\mathrm{LH2}}}{D_{\mathrm{VCS}}}(Re_{\mathrm{LH2}} * Pr_{\mathrm{LH2}}\frac{D_{\mathrm{VCS}}}{l_{\mathrm{LH2}}})^{1/3}\left(\frac{\mu_{\mathrm{LH2}}}{\mu_w}\right)^{0.14} \quad (35)$$

where λ_{LH2} is the thermal conductivity of liquid hydrogen, W/m·K; Pr_{LH2} is the liquid hydrogen's Prandtl number in VCS heat exchanger tube; Re_{LH2} is the liquid hydrogen's Reynolds number in VCS heat exchanger tube; l_{LH2} is the length of the heat exchanger tube in which the liquid hydrogen is involved in the heat exchange, m. μ_{LH2} is the dynamic viscosity of the liquid hydrogen in the VCS, Pa·s; μ_w is the dynamic viscosity of liquid hydrogen at wall temperature, Pa·s. Here the liquid hydrogen is heated, so $\left(\frac{\mu_{\mathrm{LH2}}}{\mu_w}\right)^{0.14}$ is taken to be 1.05.

As for the calculation of heat transfer for cryogenic hydrogen gas, this can be done using section 1.5.

4.7 Model Validation

The conclusions of Jiang et al. [61] on the liquid hydrogen-oxygen pair storage combined with Multi-layer Insulation (MLI) and SVCS have been used to verify the thermodynamic model in this research. They installed the VCS at 50% of the MLI and used the self-evaporating hydrogen from the liquid hydrogen tank to insulate the tank. Table 4 shows the physical parameters of the model they researched. As shown in Figure 7, the red curve represents the temperature distribution result calculated using the thermodynamic model develop in this research, while the purple stars represent the research results of Jiang et al. The average deviation of the temperature curve inside the insulation structure is only 3.2%. It is demonstrated that the calculated value of the developed model is in consistent with the research of Jiang et al. Therefore, the model developed in this research can be applied to analyse and optimize the design of the VCS used in the insulation system of the liquid hydrogen transport tank.

Table 4 The physical parameters of the model that Jiang et al. researched.

Name	Parameters	Values
Tank	Shape	cylinder
	Height	3.05 m
	Diameter	3.05 m
	Head type	2:1 elliptical dome
MLI	Low density	8 layers/cm (10 layers)
	Medium density	12 layers/cm (15 layers)
	High density	16 layers/cm (20 layers)
	Total layers	45 layers
VCS	VCS shield area of liquid hydrogen tank	34.78 m^2
	VCS tube length of liquid hydrogen tank	52.19 m
	VCS shield area of liquid oxygen tank	21.35 m^2
	VCS tube length of liquid oxygen tank	30.04 m

Inner diameter of the VCS tube	11.7 mm
VCS tube wall thickness	0.5 mm
VCS shield wall thickness	0.1 mm

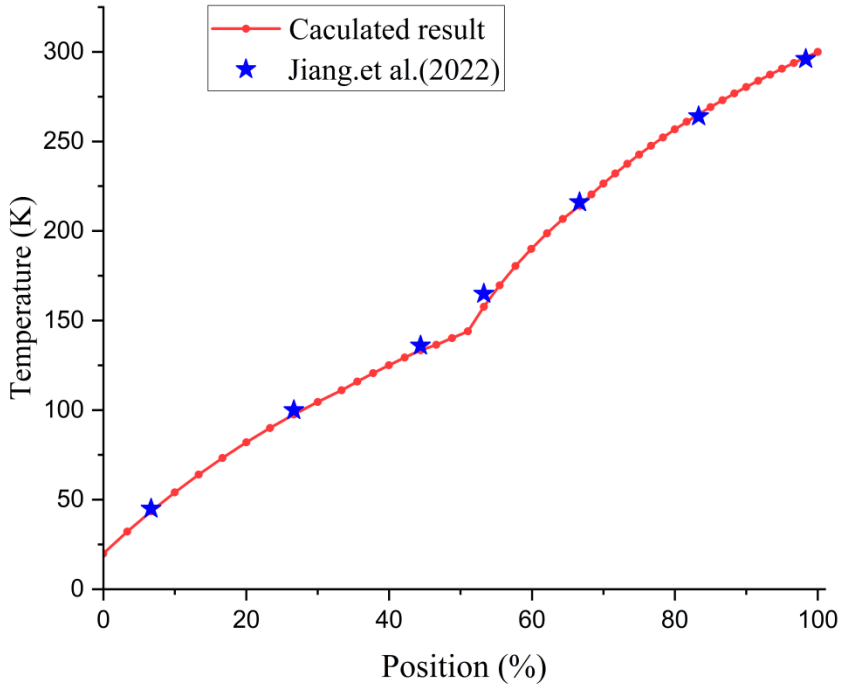

Figure 7 The comparison of the calculation results of the thermodynamic model in this research and the research results of Jiang et al.

5 Calculation Results and Discussion

5.1 Calculation Results

The VCS is embedded within the RPF and plays a function of insulation for heat transfer from tank surrounding to the hydrogen inside the tank. The amount of heat transferred to the liquid hydrogen changes with the position of the VCS within the insulation. As for the position of the VCS, the 0% mark denotes the coldest end of the insulation that is in contact with the primary shell, and 100% represents the hottest end of the insulation in contact with the secondary shell.

The thickness of the RPF is taken to be 1.84 m for an insulated structure installed with VCS. This thickness is derived from the calculation of a single RPF meeting 0.1% boil-off rate of the total mass of liquid hydrogen per day in the tank.

Figure 8 shows the relationship between the heat transferred to the liquid hydrogen in the tank and the position of the SVCS. As the installation position of SVCS moves from the primary shell to the secondary shell (0%→100%), the heat transferred to the liquid hydrogen decreases, then increases; the total heat transfer from the tank surrounding and the heat absorbed by the SVCS are increasing all the time.

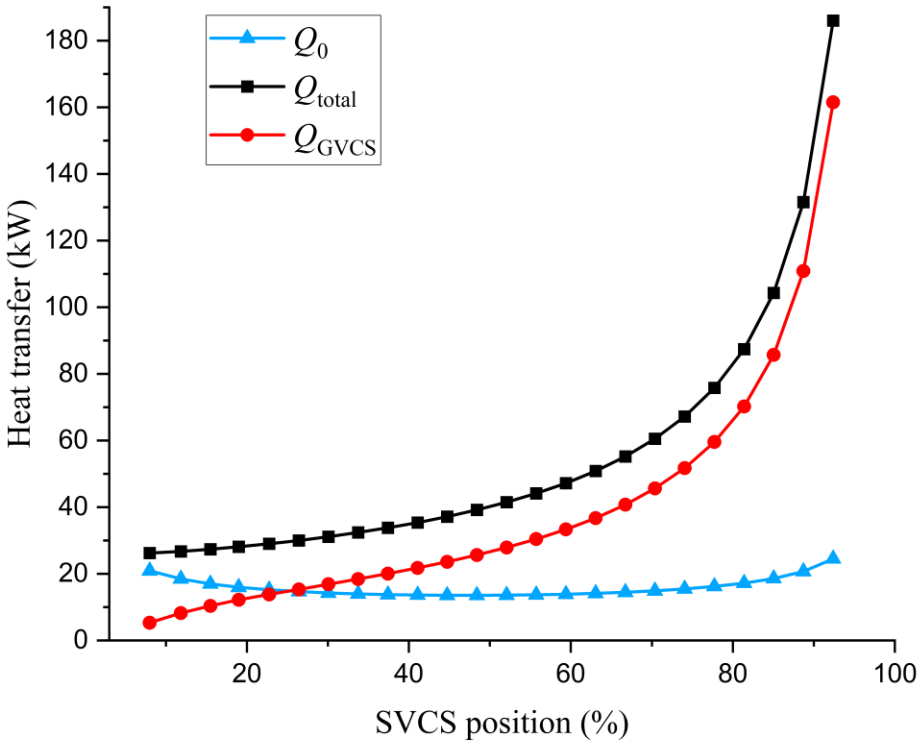

Figure 8 Relationship between heat transfer and SVCS position.

Figure 9 depicts the relationship between the position of the FVCS with cryogenic hydrogen gas in the RPF and the heat transfer to the liquid hydrogen in the tank. The heat transferred to the liquid hydrogen decreases as the FVCS+GH_2 moves from the primary shell to the secondary shell, and then increases again; the total heat transfer from the tank surrounding and the heat absorbed by the FVCS+GH_2 are increasing all the time.

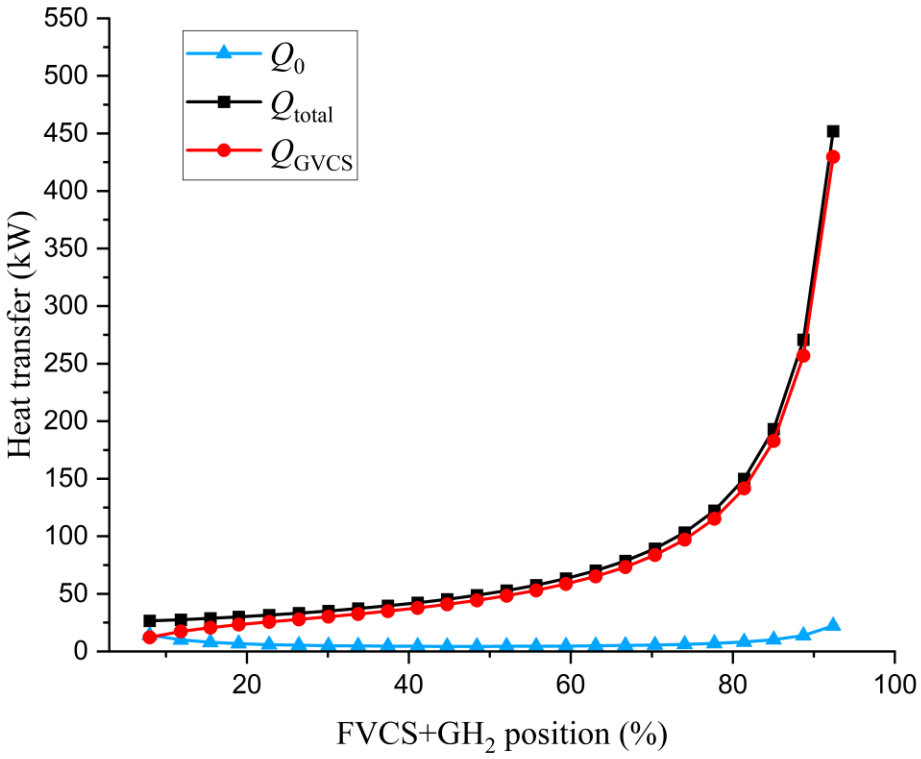

Figure 9 Relationship between heat transfer and the position of the FVCS with cryogenic hydrogen gas.

Figure 10 depicts the relationship between the position of the FVCS with cryogenic liquid hydrogen in the RPF and the heat transfer to the liquid hydrogen in the tank. The total heat transfer around the tank and the heat absorbed by the FVCS+LH_2 keeps increasing as the FVCS+LH_2 moves from the primary to the secondary shell. It should be noted that as the FVCS+LH_2 moves from 0% to 60%, the amount of heat transfer into the liquid hydrogen tank is zero and the heat transfer from the outside environment is completely absorbed by the FVCS heat exchanger tubes. This is because the heat absorbed by the liquid hydrogen in the heat exchanger tubes during this phase fails to reach the latent heat of vaporisation

value of the liquid hydrogen and the hydrogen in the tubes remains in a liquid state. The wall temperature of the heat exchanger tubes is kept at 20 K, with no temperature difference from the primary shell, and no heat transfer occurs. As the FVCS+LH_2 moves from 60% to 100%, the liquid hydrogen is heated for a period of time in the heat exchanger tubes and then evaporates into gaseous hydrogen. The gaseous hydrogen continues to participate in the heat exchange inside the tubes, but is unable to absorb all the heat transfer from the tank surrounding.

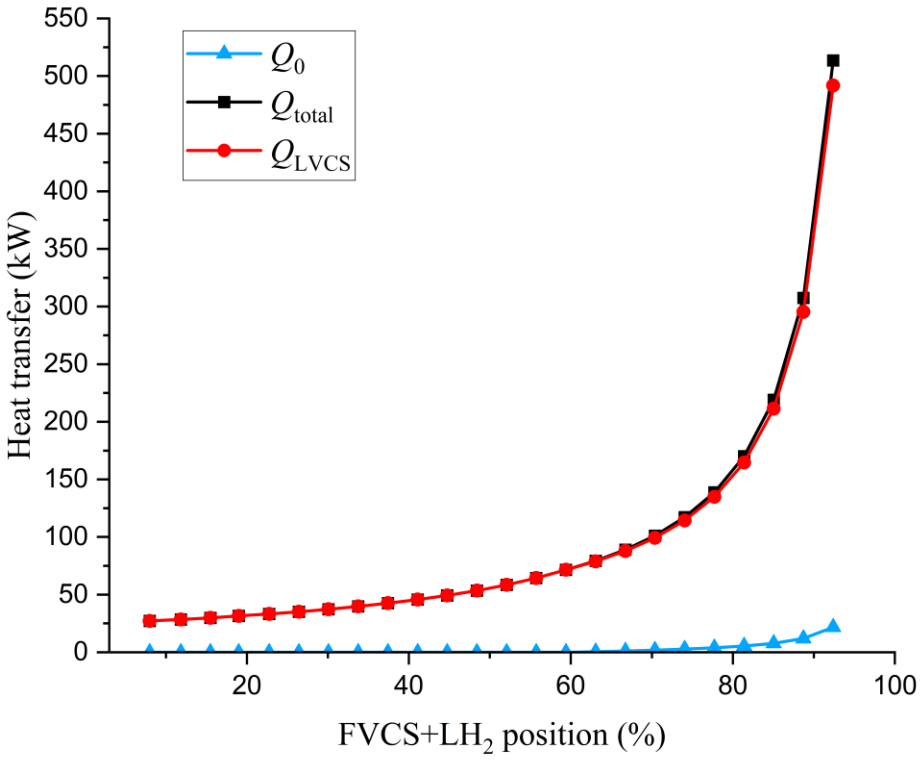

Figure 10 Relationship between heat transfer and the position of the FVCS with cryogenic liquid hydrogen.

Figure 11 depicts relationship between heat transfer Q_0 and VCS position for the four insulation structures. The single RPF has a fixed thickness and no VCS, so the heat transfer does not change. The insulation structures installed with SVCS and FVCS+GH_2, have a very strong insulation effect, and both achieve the best insulation at 50% of the insulation layer.

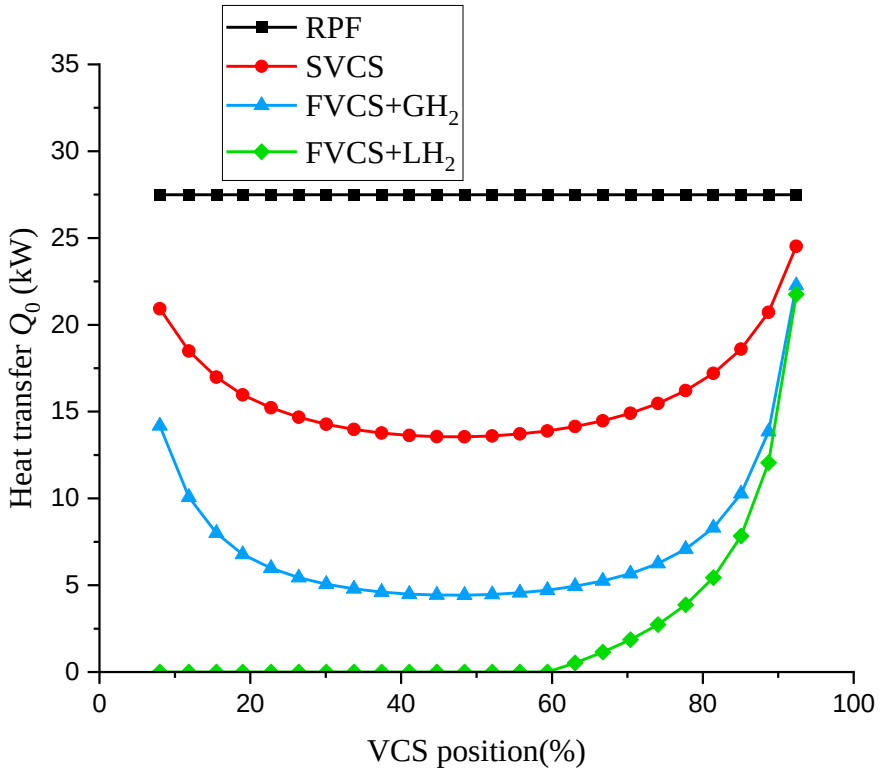

Figure 11 Relationship between heat transfer Q_0 and VCS position for the four insulation structures.

Figure 12 depicts the effect of changes in the position of the VCS on the temperature of the outermost surface of the tank T_2 and the temperature of the wall of the VCS heat exchanger tube T_{VCS}. As the VCS moves from the primary shell to the secondary shell, the

temperature of the outermost surface of the tank decreases, leading to an increase in heat transferred from the tank surrounding to the liquid hydrogen transport tank. Additionally, as the VCS is positioned closer to the outermost surface of the tank, the temperature of the VCS tends to increase and the temperature of the outermost surface of the tank tends to decrease, exacerbating the impact of the tank surrounding on the heat transfer of the liquid hydrogen transport tank. By comparing Figure 12 (a), (b) and (c), it is clear that the influence of SVCS, FVCS+GH_2 and FVCS+LH_2 on the temperature of the outermost surface of the liquid hydrogen transport tank is progressively greater.

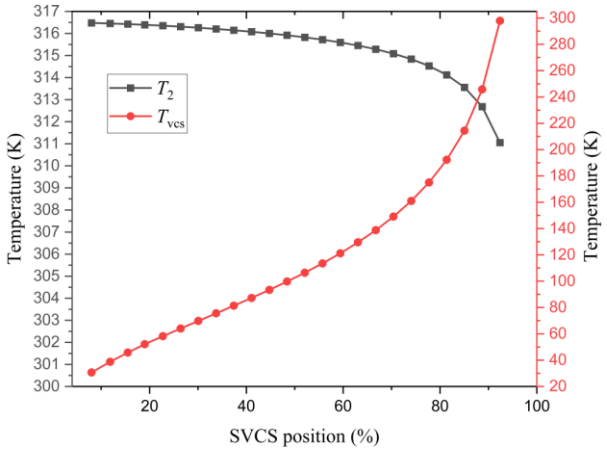

(a)

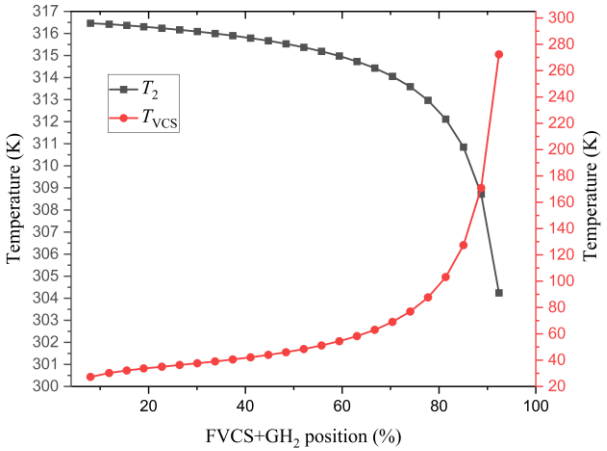

(b)

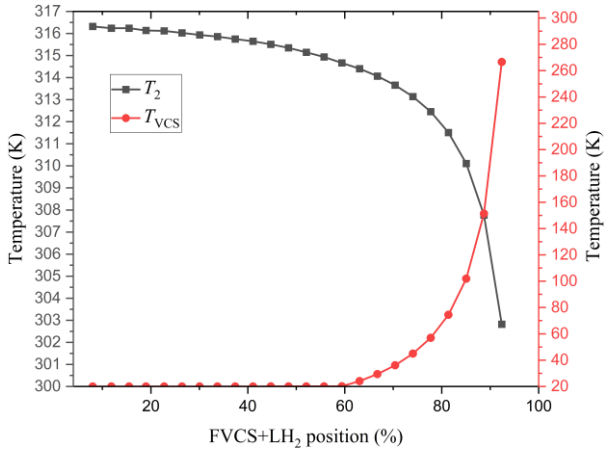

(c)

Figure 12 The effect of VCS position changes on T_2 and T_{VCS}.

Figure 13 depicts the temperature profile inside the insulation layer when the SVCS, FVCS+GH_2 and FVCS+LH_2 are installed at 50% of the insulation layer. In this case, both SVCS and FVCS+GH_2 are installed in the optimum position. Comparing the four curves, the insulation layers with VCS have significant temperature variations at the VCS installation position compared to the insulation layer with a single RPF, indicating that VCS has a significant impact on heat transfer within the insulation layer. Similarly, when comparing the SVCS and FVCS+GH_2 (they are fed with cryogenic hydrogen gas), the temperature variation of the FVCS+GH_2 is more pronounced, indicating that the FVCS+GH_2 has a greater impact on heat transfer.

Engineering practice has always expected low cost, lightweight, and simple structure implementation. In this research, two optimization design schemes for reducing the evaporation of liquid hydrogen and the thickness of the insulation layer are proposed by studying the influence of the VCS position on the heat ingress of the storage tank.

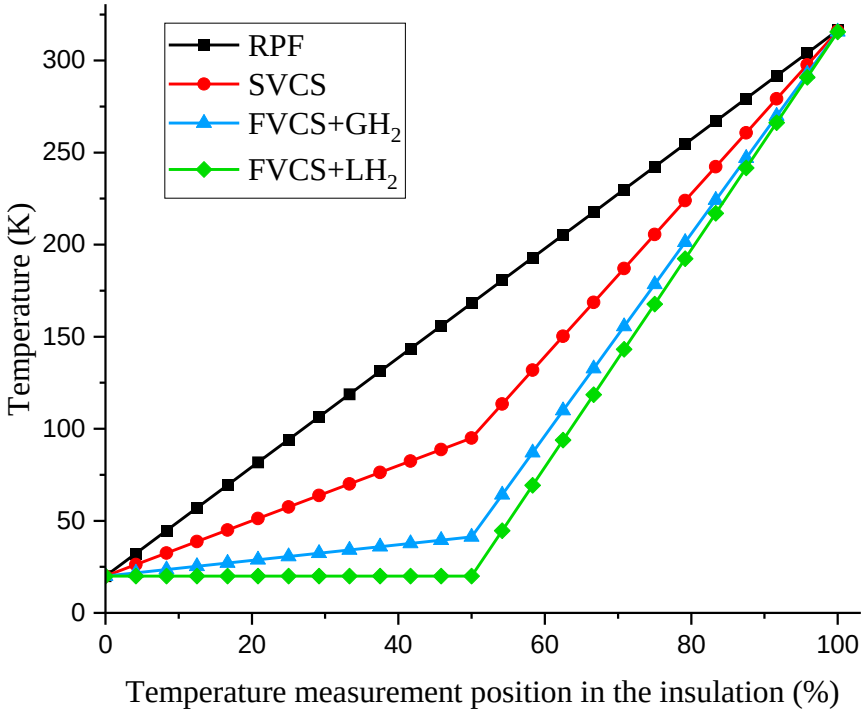

Figure 13 Temperature distribution inside the three insulation structures when the VCS is installed in the 50% of the insulation.

5.2 Optimization Scheme 1

Figure 11 shows the relationship between the heat transferred to the liquid hydrogen inside tank and the position of the VCS heat exchanger tubes, after the thickness has been fixed to be 1.84 m.

The heat transfer of the SVCS installed at 50% of the insulation is the lowest. Relative to the boil-off rate of 0.1% of the total daily mass of liquid hydrogen in the tank, it can reduce heat transfer by 47.84% in the tank and save 2,392 kg of liquid hydrogen on board per day.

The heat transfer of the FVCS installed at 50% is the lowest. Relative to the boil-off rate of 0.1% of the total daily mass of liquid hydrogen in the tank, it can reduce heat transfer by 85.86% in the tank and saving 4,293 kg of liquid hydrogen on board per day.

By installing VCS at an optimal position, the loss during the transportation of liquid hydrogen can be effectively reduced.

5.3 Optimization Scheme 2

When the daily boil-off rate of liquid hydrogen is fixed 0.1%, the thickness of the insulation can be reduced by installing SVCS and FVCS+GH_2, it results in reduced thickness of insulation layer of RPF. Figure 11 shows that the heat ingress is minimized when SVCS and FVCS+GH_2 are respectively positioned at 50% of the insulation layer.

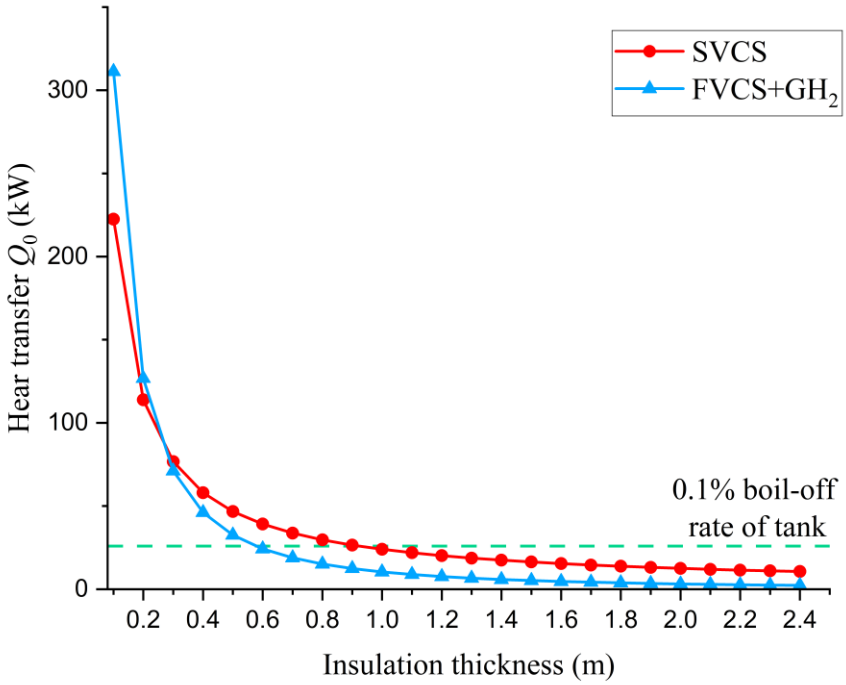

Figure 14 The effect of insulation thickness on the heat transfer Q_0 when the VCS is installed in the 50% of the insulation.

As shown in Figure 14, by installing SVCS, the RPF insulation layer only needs to be 0.92 m. Relative to the insulation of a single RPF with an installed thickness of 1.84m, this

scheme reduces the thickness of the insulation layer by 0.92 m (50%) compared to a single RPF insulation layer.

As shown in Figure 14, by installing FVCS+GH_2, the RPF insulation layer only needs to be 0.59 m. Relative to the insulation of a single RPF with an installed thickness of 1.84m, this scheme reduces the thickness of the insulation layer by 1.25 m (67.93%) compared to a single RPF insulation layer.

6 Conclusions

This research designed a large type-C tank for transporting liquid hydrogen by ships, calculated the shell thickness, selected the shell material and proposed four insulation strategies. The performances of the four insulation layers: RPF, Self-evaporation Vapor-Cooled Shield (SVCS), Forced-evaporation Vapor-Cooled Shield with cryogenic hydrogen gas (FVCS+ GH_2) and Forced-evaporation Vapor-Cooled Shield with liquid hydrogen (FVCS+ LH_2) are investigated using thermodynamic models, include the effect of the VCS position on heat transfer and temperature distribution in the insulation layer. Furthermore, the optimal positions of the VCS in the insulation are identified, and two different optimization schemes are proposed based on the research findings. Major conclusive remarks are presented as follows:

(1) The thickness of the primary shell and secondary shell are designed to be 47.70 mm, and AISI type 316L Stainless Steel (annealed plate) is chosen as their material.

(2) Installing VCS in the insulation layer can significantly reduce heat transfer to the liquid hydrogen inside the tank. The heat transfer to the liquid hydrogen decreases and then increases as the VCS moves from the from the primary shell to the secondary shell (0%→ 100%) in the insulation layer. The optimal heat transfer position for SVCS and FVCS+ GH_2 both are 50%.

(3) An optimized scheme for reducing liquid hydrogen evaporation loss is investigated. As stated above, when the thickness of the insulation layer remains constant, installing the

SVCS at 50% of the insulation layer can reduce heat transfer by 47.84% in the tank and save 2,392 kg of liquid hydrogen on board per day; installing the FVCS+ GH_2 at 50% of the insulation layer can reduce heat transfer by 85.86% in the tank and saving 4,293 kg of liquid hydrogen on board per day. This optimization scheme can significantly reduce liquid hydrogen boil-off rate during ship transportation.

(4) An optimized scheme for the thickness of the insulation layer is designed. When satisfying the boil-off rate of liquid hydrogen to be less than 0.1% per day, installing SVCS at 50% of the insulation layer can reduce the thickness of the insulation layer by 0.92 m (50%) compared to a single RPF insulation layer; installing FVCS+ GH_2 at 50% of the insulation layer can reduce the thickness by 1.25 m (67.93%). This optimized scheme can effectively reduce transportation tank's volume and weight while also reducing construction costs.

Prospects: This research focuses on the use of C-tanks for storing and transporting liquid hydrogen. In the future there are still many topics that need to be investigated. For example, in the area of insulation, the economic use of vacuum insulation for the transport of liquid hydrogen can be investigated. In terms of the type of tank, the use of membrane tanks for the transport of liquid hydrogen could be investigated. In short, more research needs to be devoted to the study of the transport of liquid hydrogen by ship.

Reference

[1] The 27th Conference of the Parties of the UNFCCC, https://unfccc.int/event/cop-27; 2022.
[2] Van Hoecke L, Laffineur L, Campe R, Perreault P, Verbruggen SW, Lenaerts S. Challenges in the use of hydrogen for maritime applications. Energy & Environmental Science. 2021;14:815-43. https://doi.org/10.1039/D0EE01545H.
[3] Fetting C. The European Green Deal. ESDN Report, December. 2020.
[4] Hydrogen roadmap Europe: a sustainable pathway for the European energy transition, https://www.h2knowledgecentre.com/content/researchpaper1125; 2019.
[5] Burhan M, Shahzad MW, Oh SJ, Ng KC. A pathway for sustainable conversion of sunlight to hydrogen using proposed compact CPV system. Energy conversion and management. 2018;165:102-12. https://doi.org/10.1016/j.enconman.2018.03.027.
[6] Yılmaz İ, İlbaş M, Taştan M, Tarhan C. Investigation of hydrogen usage in aviation industry. Energy conversion and management. 2012;63:63-9.
[7] Cau G, Cocco D, Petrollese M, Kær SK, Milan C. Energy management strategy based on short-term generation scheduling for a renewable microgrid using a hydrogen storage system. Energy Conversion and Management. 2014;87:820-31. https://doi.org/10.1016/j.enconman.2014.07.078.
[8] Scita R, Raimondi PP, Noussan M. Green hydrogen: the holy grail of decarbonisation? An analysis of the technical and geopolitical implications of the future hydrogen economy. 2020. https://dx.doi.org/10.2139/ssrn.3709789.
[9] Fesmire J. Research and Development History of Glass Bubbles Bulk-Fill Thermal Insulation Systems for Large-Scale Cryogenic Liquid Hydrogen Storage Tanks. 2017. https://ntrs.nasa.gov/citations/20180006604.
[10] Zheng J, Chen L, Wang J, Zhou Y, Wang J. Thermodynamic modelling and optimization of self-evaporation vapor cooled shield for liquid hydrogen storage tank. Energy Conversion and Management. 2019;184:74-82. https://doi.org/10.1016/j.enconman.2018.12.053.
[11] Sinigaglia T, Lewiski F, Martins MES, Siluk JCM. Production, storage, fuel stations of hydrogen and its utilization in automotive applications-a review. International journal of hydrogen energy. 2017;42:24597-611. https://doi.org/10.1016/j.ijhydene.2017.08.063.
[12] Fesmire J, Swanger A, Jacobson J, Notardonato W. Energy efficient large-scale storage of liquid hydrogen. IOP Conference Series: Materials Science and Engineering: IOP Publishing; 2022. p. 012088. https://iopscience.iop.org/article/10.1088/1757-899X/1240/1/012088/meta.
[13] Kick start for new clean energy trade. The Motorship, https://www.motorship.com/vessels-and-shipyards/kick-start-for-new-clean-energy-trade/1352971.article; 2020.
[14] SAFETY REQUIREMENTS FOR CARRIAGE OF LIQUEFIED HYDROGEN IN BULK. IMO; 2016.
[15] Park H, Kim J, Bergan PG, Chang D. Structural design of flexible vacuum insulation system for large-scale LH2 storage. International Journal of Hydrogen Energy. 2022;47:39179-92. https://doi.org/10.1016/j.ijhydene.2022.09.063.
[16] Alkhaledi AN, Sampath S, Pilidis P. A hydrogen fuelled LH2 tanker ship design. Ships and Offshore Structures. 2022;17:1555-64. https://doi.org/10.1080/17445302.2021.1935626.
[17] Revision of the interim recommendations for carriage of liquefied hydrogen in bulk. IMO; 2021.
[18] Guo Y, Lin G, He J, Bai L, Zhang H, Miao J. Experimental study on the supercritical startup and heat transport capability of a neon-charged cryogenic loop heat pipe. Energy Conversion and Management. 2017;134:178-87. https://doi.org/10.1016/j.enconman.2016.12.038.
[19] Dye S, Johnson W, Plachta D, Mills G, Buchanan L, Kopelove A. Design, fabrication and test of Load Bearing multilayer insulation to support a broad area cooled shield. Cryogenics. 2014;64:135-40. https://doi.org/10.1016/j.cryogenics.2014.06.001.
[20] Zheng J, Chen L, Cui C, Guo J, Zhu W, Zhou Y, et al. Experimental study on composite insulation system of spray on foam insulation and variable density multilayer insulation. Applied Thermal Engineering. 2018;130:161-8. https://doi.org/10.1016/j.applthermaleng.2017.11.050.

[21] Carriço CS, Fraga T, Carvalho VE, Pasa VM. Polyurethane foams for thermal insulation uses produced from castor oil and crude glycerol biopolyols. Molecules. 2017;22:1091. https://doi.org/10.3390/molecules22071091.
[22] Kang D, Yun S, Kim B-k. Review of the Liquid Hydrogen Storage Tank and Insulation System for the High-Power Locomotive. Energies. 2022;15:4357. https://doi.org/10.3390/en15124357.
[23] Konieczny A, Mondal K, Wiltowski T, Dydo P. Catalyst development for thermocatalytic decomposition of methane to hydrogen. International Journal of Hydrogen Energy. 2008;33:264-72. https://doi.org/10.1016/j.ijhydene.2007.07.054.
[24] Ashik U, Viswan A, Kudo S, Hayashi J-i. Nanomaterials as catalysts. Applications of Nanomaterials: Elsevier; 2018. p. 45-82.
[25] Parsapur RK, Chatterjee S, Huang K-W. The insignificant role of dry reforming of methane in CO2 emission relief. ACS Energy Letters. 2020;5:2881-5. https://doi.org/10.1021/acsenergylett.0c01635.
[26] Buttler A, Spliethoff H. Current status of water electrolysis for energy storage, grid balancing and sector coupling via power-to-gas and power-to-liquids: A review. Renewable and Sustainable Energy Reviews. 2018;82:2440-54. https://doi.org/10.1016/j.rser.2017.09.003.
[27] Esposito DV. Membraneless electrolyzers for low-cost hydrogen production in a renewable energy future. Joule. 2017;1:651-8. https://doi.org/10.1016/j.joule.2017.07.003.
[28] Parkinson B, Balcombe P, Speirs J, Hawkes A, Hellgardt K. Levelized cost of CO 2 mitigation from hydrogen production routes. Energy & environmental science. 2019;12:19-40. https://doi.org/10.1039/C8EE02079E.
[29] Wang Z, Wang Y, Afshan S, Hjalmarsson J. A review of metallic tanks for H2 storage with a view to application in future green shipping. International Journal of Hydrogen Energy. 2021;46:6151-79. https://doi.org/10.1016/j.ijhydene.2020.11.168.
[30] Zheng J, Chen L, Xu X, Guo L, Zhou Y, Wang J. A novel insulation system based on active cooling without power input for liquid hydrogen storage. Energy. 2019;182:1-10. https://doi.org/10.1016/j.energy.2019.06.050.
[31] Foster SL, Bakovic SIP, Duda RD, Maheshwari S, Milton RD, Minteer SD, et al. Catalysts for nitrogen reduction to ammonia. Nature Catalysis. 2018;1:490-500. https://doi.org/10.1038/s41929-018-0092-7.
[32] Aakko-Saksa PT, Cook C, Kiviaho J, Repo T. Liquid organic hydrogen carriers for transportation and storing of renewable energy–Review and discussion. Journal of Power Sources. 2018;396:803-23. https://doi.org/10.1016/j.jpowsour.2018.04.011.
[33] Netskina O, Tayban E, Prosvirin I, Komova O, Simagina V. Hydrogen storage systems based on solid-state NaBH4/Co composite: Effect of catalyst precursor on hydrogen generation rate. Renewable Energy. 2020;151:278-85. https://doi.org/10.1016/j.renene.2019.11.031.
[34] Kumar R, Karkamkar A, Bowden M, Autrey T. Solid-state hydrogen rich boron–nitrogen compounds for energy storage. Chemical Society Reviews. 2019;48:5350-80. https://doi.org/10.1039/C9CS00442D.
[35] Tietze V, Luhr S, Stolten D. Bulk storage vessels for compressed and liquid hydrogen. Hydrogen science and engineering: materials, processes, systems and technology. 2016:659-90. https://doi.org/10.1002/9783527674268.ch27.
[36] Gillette J, Kolpa R. Overview of interstate hydrogen pipeline systems. Argonne National Lab.(ANL), Argonne, IL (United States); 2008. https://doi.org/10.2172/924391.
[37] Ball M, Weeda M. The hydrogen economy–vision or reality? International Journal of Hydrogen Energy. 2015;40:7903-19. https://doi.org/10.1016/j.ijhydene.2015.04.032.
[38] Mansilla C, Bourasseau C, Cany C, Guinot B, Le Duigou A, Lucchese P. Hydrogen applications: Overview of the key economic issues and perspectives. Hydrogen Supply Chains. 2018:271-92. https://doi.org/10.1016/B978-0-12-811197-0.00007-5.
[39] Tarkowski R. Underground hydrogen storage: Characteristics and prospects. Renewable and Sustainable Energy Reviews. 2019;105:86-94. https://doi.org/10.1016/j.rser.2019.01.051.
[40] Amos WA. Costs of storing and transporting hydrogen. National Renewable Energy Lab.(NREL), Golden, CO (United States); 1999. https://doi.org/10.2172/6574.
[41] Hart D. Hydrogen Power: The Commercial Future of'the Ultimate Fuel': Financial Times Energy Publ.; 1997.

[42] Timmerhaus KD, Flynn TM. Cryogenic process engineering: Springer Science & Business Media; 2013.
[43] Fesmire J, Sass J, Nagy Z, Sojourner S, Morris D, Augustynowicz S. Cost-efficient storage of cryogens. AIP Conference Proceedings: American Institute of Physics; 2008. p. 1383-91. https://doi.org/10.1063/1.2908498.
[44] Everitt C, Parmley R, Taber M, Bencze W, Burns K, Frank D, et al. Gravity Probe B cryogenic payload. Classical and Quantum Gravity. 2015;32:224009. DOI 10.1088/0264-9381/32/22/224009.
[45] Fujimoto R, Mitsuda K, Yamasaki N, Takei Y, Tsujimoto M, Sugita H, et al. Cooling system for the soft X-ray spectrometer onboard Astro-H. Cryogenics. 2010;50:488-93. https://doi.org/10.1016/j.cryogenics.2010.02.004.
[46] Fujimoto R, Mitsuda K, Hirabayashi M, Narasaki K, Breon S, Boyle R, et al. Neon dewar for the X-ray spectrometer onboard Suzaku. Nuclear Instruments and Methods in Physics Research Section A: Accelerators, Spectrometers, Detectors and Associated Equipment. 2006;559:648-50. https://doi.org/10.1016/j.nima.2005.12.093.
[47] Le Bar J, Cady E. The advanced cryogenic evolved stage (ACES)-a low-cost, low-risk approach to space exploration launch. Space 20062006. p. 7454.
[48] Mozah: Samsung's contribution to the Q-max LNG tanker series. Significant Ships of 2008, 2008.
[49] Duthil P. Material properties at low temperature. arXiv preprint arXiv:150107100. 2015. https://doi.org/10.48550/arXiv.1501.07100.
[50] Song J, Curtin W. Atomic mechanism and prediction of hydrogen embrittlement in iron. Nature materials. 2013;12:145-51. https://doi.org/10.1038/nmat3479.
[51] Gangloff RP, Somerday BP. Gaseous hydrogen embrittlement of materials in energy technologies: the problem, its characterisation and effects on particular alloy classes: Elsevier; 2012.
[52] Dwivedi SK, Vishwakarma M. Hydrogen embrittlement in different materials: A review. International Journal of Hydrogen Energy. 2018;43:21603-16. https://doi.org/10.1016/j.ijhydene.2018.09.201.
[53] Park WS, Yoo SW, Kim MH, Lee JM. Strain-rate effects on the mechanical behavior of the AISI 300 series of austenitic stainless steel under cryogenic environments. Materials & Design. 2010;31:3630-40. https://doi.org/10.1016/j.matdes.2010.02.041.
[54] Qiu Y, Yang H, Tong L, Wang L. Research progress of cryogenic materials for storage and transportation of liquid hydrogen. Metals. 2021;11:1101. https://doi.org/10.3390/met11071101.
[55] DeSisto TS, Carr L. Low temperature mechanical properties of 300 series stainless steel and titanium. Advances in Cryogenic Engineering: Proceedings of the 1960 Cryogenic Engineering Conference University of Colorado and National Bureau of Standards Boulder, Colorado August 23–25, 1960: Springer; 1961. p. 577-86.
[56] AISI Type 316L Stainless Steel, annealed plate. https://asm.matweb.com/search/SpecificMaterial.asp?bassnum=mq316p.
[57] SOCIETY CC. RULES FOR CONSTRUCTION AND EQUIPMENT OF SHIPS CARRYING LIQUEFIED GASES IN BULK. 2022. p. 49-53.
[58] International Code for the Construction and Equipment of Ships Carrying Liquefied Gases in Bulk. International Maritime Organization (IMO); 2016..
[59] Bergman TL, Lavine AS, Incropera FP, DeWitt DP. Introduction to heat transfer: John Wiley & Sons; 2011, p.136-585.
[60] Sieder EN. Heat transfer and pressure drop of liquids in tubes. Industrial & Engineering Chemistry 2812 (1936). 1936:1429-35. https://pubs.acs.org/doi/pdf/10.1021/ie50324a027?casa_token=PhB_i2W-MUIAAAAA:68R4z5KAWfDU0Wj2OK6wcL8S22jwWpyxJzBdavSQhXj8-sKKHKzqKu_Deqr-PgsmoRn6BwWSXjNBi6Ej
[61] Jiang W, Zuo Z, Sun P, Li P, Huang Y. Thermal analysis of coupled vapor-cooling-shield insulation for liquid hydrogen-oxygen pair storage. International Journal of Hydrogen Energy. 2022;47:8000-14. https://doi.org/10.1016/j.ijhydene.2021.12.103.
[62] M.E. Demir, I. Dincer. Cost assessment and evaluation of various hydrogen delivery scenarios. Int J Hydrogen Energy, 43 (2018), pp. 10420-10430. https://doi.org/10.1016/j.ijhydene.2017.08.002.
[63] R. Gerboni. Introduction to hydrogen transportation. Compend. Hydrog. Energy (2016), pp. 283-299. https://doi.org/10.1016/b978-1-78242-362-1.00011-0.
[64] Faye O, Szpunar J, Eduok U. A critical review on the current technologies for the generation, storage,

and transportation of hydrogen. International Journal of Hydrogen Energy, 2022, 47(29): 13771-13802. https://doi.org/10.1016/j.ijhydene.2022.02.112.
[65] d'Amore-Domenech R, Meca V L, Pollet B G, et al. On the bulk transport of green hydrogen at sea: Comparison between submarine pipeline and compressed and liquefied transport by ship. Energy, 2023, 267: 126621. https://doi.org/10.1016/j.energy.2023.126621.
[66] Finance B N E. Hydrogen–the economics of production from renewables[R]. full report. Technical Report. Bloomberg, 2020.